High-efficiency, low-voltage phosphorescent organic light-emitting diode devices with mixed host

Marina E. Kondakova, Thomas D. Pawlik, Ralph H. Young, David J. Giesen, Denis Y. Kondakov, Christopher T. Brown, Joseph C. Deaton, Jerome R. Lenhard, and Kevin P. Klubek

Citation: Journal of Applied Physics **104**, 094501 (2008); doi: 10.1063/1.3000046
View online: http://dx.doi.org/10.1063/1.3000046
View Table of Contents: http://scitation.aip.org/content/aip/journal/jap/104/9?ver=pdfcov
Published by the AIP Publishing

High-efficiency, low-voltage phosphorescent organic light-emitting diode devices with mixed host

Marina E. Kondakova,[a] Thomas D. Pawlik, Ralph H. Young, David J. Giesen, Denis Y. Kondakov, Christopher T. Brown,[b] Joseph C. Deaton, Jerome R. Lenhard, and Kevin P. Klubek
Eastman Kodak Company, Rochester, New York 14650-2103, USA

(Received 18 April 2008; accepted 25 August 2008; published online 4 November 2008)

We report high-efficiency, low-voltage phosphorescent green and blue organic light-emitting diode (PHOLED) devices using mixed-host materials in the light-emitting layer (LEL) and various combinations of electron-injecting and electron-transporting layers. The low voltage does not rely on doping of the charge-transport layers. The mixed LEL architecture offers significantly improved efficiency and voltage compared to conventional PHOLEDs with neat hosts, in part by loosening the connection between the electrical band gap and the triplet energy. Bulk recombination in the LEL occurs within ~10 nm of the interface with an electron-blocking layer. A "hole-blocking layer" need not have hole- or triplet-exciton-blocking properties. Optical microcavity effects on the spectrum and efficiency were used to locate the recombination zone. The effect of layer thickness on drive voltage was used to determine the voltage budget of a typical device. The behavior of undoped devices was investigated, and the electroluminescence is attributed to an exciplex of the two host materials. Electrically detected electron paramagnetic resonance was used to study the behavior of doped and undoped PHOLED devices from 20 to 200 K, which largely mimics the behavior of the same devices at room temperature. © *2008 American Institute of Physics*.
[DOI: 10.1063/1.3000046]

I. INTRODUCTION

Because of their very high external quantum efficiencies (EQEs),[1] phosphorescent organic light-emitting diodes (PHOLEDs) have been a subject of intense research and development activity. The higher quantum efficiency leads to reduced power consumption, relative to conventional fluorescent OLEDs (FOLEDs), which is critical for application in full-color OLED displays. White OLED devices incorporating phosphorescent light-emitting layers are currently under development for solid-state lighting applications. The operating lifetimes of PHOLEDs, often greatly inferior to those of FOLEDs, are a limiting factor in potential applications.

Conventional FOLED devices generally contain at least three layers—hole-transporting, light-emitting, and electron-transporting layers (HTL, LEL, and ETL)—placed between the anode and the cathode. Additional layers may be used to modify the anode and cathode while maintaining the central three-layer structure responsible for the electroluminescence (EL). Extremely high efficiencies have been reported for PHOLEDs of this structure; the operating lifetime, however, has not been reported.[2,3] For the best performance, PHOLED structures typically require additional layers, such as charge-blocking and exciton-confining layers between the LEL and the HTL and/or the ETL.[4–8] Very efficient PHOLEDs with a double LEL (D-LEL) and *p*- and *n*-doped charge-transporting layers have been demonstrated.[9,10] The materials of the two LELs usually carry only holes or electrons, respectively. Hence, much of the recombination in these devices probably occurs exactly at the junction between the two LELs. This feature may adversely affect the device lifetime because a few molecules are responsible for generating excited states and, simultaneously, bear the brunt of any recombination-related degradation processes. This problem may be alleviated, in principle, by using a distributed interface with graded light-emitting and/or charge-transporting layers. Graded charge-transporting layers reportedly improve the operational lifetime of certain fluorescent devices,[11] but we are unaware of detailed investigations of this OLED architecture. Improvement of luminous yield has been observed for certain blue PHOLEDs with a graded LEL, but operating lifetimes were not reported.[12]

It is widely believed that a broad recombination zone is advantageous for luminous efficiency and operating lifetime.[13–15] It requires a LEL that transports both electrons and holes. The host may be a single bipolar material[14,16] or a mixture of electron- and hole-transporting compounds. (An alternative device concept is to use a phosphorescent dopant in the LEL at sufficient concentration to transport electrons and/or holes and participate directly in the recombination process.[17]) Mixed LEL hosts have been used often in conventional FOLEDs to improve the efficiency, voltage, and operating lifetime,[18–20] but relatively little information on mixed-host PHOLEDs has been reported.[21–24] We have already demonstrated very efficient, low-voltage red and green PHOLEDs with mixed-host compositions and low-field ETL compositions.[25–27] Here we report a detailed study of this device structure and extend it to blue PHOLEDs.

In almost any OLED, the LEL consists of a host material

[a]Electronic mail: marina.kondakova@kodak.com.
[b]Present address: Plextronics, Inc., 2180 William Pitt Way, Pittsburgh, PA 15238.

and a dopant. The host is usually responsible for charge transport, and the dopant is responsible for emission of light, while the component(s) responsible for electron-hole recombination depends on the structure of the device. The properties of the host, the dopant, and the materials of adjoining layers are all critical for optimizing the device performance. In a PHOLED, it is highly preferable that the lowest triplet state of the host be energetically well above that of the dopant so that triplet excitons reside preferentially on the dopant. It can also be advantageous for the triplet states of adjoining layers to lie even higher, so that triplet excitons are confined to the LEL. Depending on their charge-injection and transport properties, recombination can occur at an interface, such as the HTL|LEL or LEL|ETL interface, or in the bulk of the LEL.

Selection of a PHOLED host material presents an intrinsic challenge. Dopants with various triplet energies are used to generate various colors of emission. As the triplet energy of the dopant increases, it becomes increasingly difficult to find suitable hosts with even higher triplet energy levels. Generally, a large triplet energy implies a large electrical band gap, i.e., a deep highest occupied molecular orbital (HOMO) and/or shallow lowest unoccupied molecular orbital (LUMO) level (large ionization potential and/or small electron affinity). A suitable single-component ("neat") host, therefore, typically presents a large barrier to injection of holes, electrons, or both. The result is a tendency to unipolar conduction and/or a high drive voltage. The root problem is that a single host material is required to do too many things. An analogous problem exists with FOLEDs, but it is much more severe for PHOLEDs. For a PHOLED host having a given triplet energy and a FOLED host having an equal singlet energy level, the PHOLED host generally has a much bigger HOMO-LUMO gap. A mixed LEL host loosens the link between transport levels and triplet energies by assigning the functions of electron and hole transport to different compounds, the two (or more) cohosts. One cohost is selected for its high triplet energy and ability to accept and transport holes from an adjacent layer, and one likewise for electrons. The materials in adjacent layers are chosen, *inter alia*, for their charge-injection properties.

II. EXPERIMENTAL METHODS

All materials were synthesized at Kodak. The PHOLEDs were fabricated on glass substrates precoated with an approximately 25 nm layer of indium tin oxide (ITO) as the anode. The substrates were scrubbed in a detergent solution, rinsed with deionized water, dried, and exposed to an oxygen plasma for approximately 1 min. Then, a 1 nm fluorocarbon (CF_x) hole-injecting layer was deposited by plasma polymerization of CHF_3 over the ITO.[28] The substrates were transferred into a vacuum chamber, and the organic layers were deposited sequentially by thermal evaporation under a vacuum of $10^{-6}-10^{-7}$ Torr. Finally, a bilayer cathode consisting of 0.5 nm of LiF, overlaid by 100 nm of aluminum, was vacuum deposited.[29,30] The device active area is 0.1 cm^2. The entire device was hermetically encapsulated, together with a desiccant, under dry nitrogen.

The EL properties of the OLEDs were evaluated using a Photoresearch PR650 SpectraScan Colorimeter and a programmable constant-current source meter at room temperature. The devices were viewed perpendicular to the device plane, and the angular distribution of the EL was assumed to be Lambertian. The drive voltages were corrected for bus resistance. Devices were aged electrically at room temperature in a standard square-wave ac mode (80 Hz, 50% duty cycle, −14 V reverse bias). The amplitude was adjusted so that the starting luminance was 1000 cd/m^2. The time required to reach 500 cd/m^2 defines the half-life t_{50}. Built-in voltages were evaluated from open-circuit photovoltage data.[31,32]

One-electron energy levels for materials of interest were estimated from redox potentials measured by cyclic voltammetry using a CHI660A electrochemical analyzer (CH Instruments, Inc., Austin TX). Solutions for voltammetry were prepared with analyte concentrations of approximately 5×10^{-4} M in acetonitrile/toluene (1:1) mixture containing $0.1M$ tetrabutylammonium tetrafluoroborate ($TBABF_4$). A glassy carbon working electrode (Bioanalytical Systems, 0.2 cm^2) was polished with alumina prior to an experiment and further polished on billiard cloth (Buehler, Metadi) saturated with acetonitrile, then rinsed with acetonitrile prior to each voltammetric scan. A Pt coil counterelectrode and a KCl-saturated calomel reference electrode were also utilized. Formal redox potentials were taken as the average of the voltammetric peak potentials for reversible electrode systems, while the peak potential obtained at a scan rate of 0.1 V/s was used as the lower limit estimate for chemically irreversible systems. Automatic iR compensation was used. Ferrocene served as an internal standard and exhibited a reproducible oxidation potential of 0.50 V in these experiments. All solutions were deaerated with argon for 15 min prior to examination.

Ultraviolet photoelectron spectra (UPS) of selected materials were obtained as described previously.[27] HOMO levels were identified with the solid-state ionization potentials (SSIPs). For eight OLED materials spanning a range of 0.7 eV, both SSIPs and reversible oxidation potentials had been collected in a uniform manner. A correlation with a slope of 1.0 and intercept of 4.45 eV was obtained, with deviations not larger than 0.09 eV (cf. Ref. 33). Therefore, HOMO and LUMO levels were (also) evaluated from the solution redox potentials by adding a constant of 4.45 eV.

Triplet energies of most materials were estimated experimentally from phosphorescence spectra at 77 K.[34] The compound of interest was dissolved in a glass-forming solvent—20% iodobenzene, 40% dichloromethane, and 40% toluene. The solution was cooled in a transparent liquid-nitrogen Dewar. It was excited with a cw source, either a xenon lamp and monochromator or a cw laser (He/Cd at 325 or 442 nm or argon ion at 364 nm), through a chopper. A grating monochromator, photomultiplier tube, and synchronized gated

TABLE I. Molecular properties. Columns 2 and 3: ionization potential (negative of HOMO energy $-E_{HOMO}$) evaluated by UPS and by electrochemistry. Column 4: electron affinity (negative of LUMO energy $-E_{LUMO}$) from electrochemistry. Columns 5 and 6: triplet energies evaluated from phosphorescence spectra and rescaled DFT computations. Electrochemical processes are reversible unless otherwise noted.

	$-E_{HOMO}$ (eV)		$-E_{LUMO}$ (eV)	E_T (eV)	
Compound	UPS	E_{ox}+4.45	E_{red}+4.45	Expt.	DFT
Alq	5.74		2.45	2.19	2.11
BAlq′	6.05		~2.5 [a]	2.31	2.21
Bphen	6.5		~2.55	2.59	2.64
CBP	6.04		2.106	2.61	2.67
NPB	5.40	5.31	2.072	2.41	2.50
PADN[b]		5.738	2.663		1.82
SBFK		>6.35 [c]	2.876	2.62	2.49
TBADN	5.65	5.704	2.533	1.81	1.86
TBP[d]		5.417	2.663		1.67
TCTA		5.517	<1.85 [e]	2.86	2.85
TPBI		~6.2 [f]	2.417	2.74	2.69
$Ir(ppy)_3$	5.18	5.218	2.185	2.49	2.54
$Ir(F_2ppy)_3$		5.679	2.381	2.71	2.85

[a]Irreversible reduction. LUMO may up to 0.3 eV higher.
[b]2-phenyl-9,10-di(2-naphthyl)anthracene.
[c]No oxidation observed within solvent window; HOMO is significantly deeper.
[d]2,5,8,11-tetra-t-butylperylene.
[e]No reduction observed within solvent window; LUMO is significantly higher.
[f]Irreversible oxidation. HOMO may be lower by as much as 0.3 eV.

photon counter were used to acquire the delayed ($\geq$200 μs) luminescence spectrum. A point on the short-wave edge of that spectrum, halfway up to the "0-0 band" maximum, was identified as the triplet energy. A more exact identification would require a bandshape analysis or a singlet-triplet absorption or excitation spectrum.[35] However, the present, simple method produces reasonable agreement with the quantum-chemically computed values (see below), providing support for both. The triplet energies of the phosphorescent dopants were obtained from absorption and emission spectra in degassed ethyl acetate solution at room temperature, replotted in a suitable fashion.[36] The wavenumber about which the absorption and emission edges exhibited (approximate) mirror symmetry was identified with the triplet energy.

Density-functional theory (DFT) was used also to calculate the energy of each molecule in its ground state (E_{S0}) and lowest triplet state (E_{T1}), with the geometry optimized for each. An empirical correlation was established between the resulting energy differences, E_{T1}-E_{S0} and the experimental triplet energies $E(T)$ of 55 molecules selected from Ref. 37,

$$E(T) = 0.84^{*}(E_{T1} - E_{S0}) + 0.35 \text{ eV}. \quad (1)$$

The average deviation is 0.13 eV. This equation was then used to refine the DFT results for the molecules in Table I. The DFT calculations used the B3LYP[38,39] functional with the GAUSSIAN98,[40] GAUSSIAN03,[41] PQS,[42] and JAGUAR[43] computer programs. The basis sets used were LACV3P[44] for Ir, 6-31G* [45,46] for Al, and MIDI![47] for all other atoms. The LACV3P pseudopotential was used for Ir atoms.

For film photoluminescence (PL) studies, ~100 nm layers of TPBI, TCTA, and a 70:30 mixture of 2,2′,2″-(1,3,5-benzenetriyl)*tris*[1-phenyl-1-H-benzimidazole] (TPBI) and 4,4′,4″-*tris*(*N*-carbazolyl)triphenylamine (TCTA) were each vacuum deposited onto CF_x-treated ITO as described above. After deposition, the films were immediately loaded into a sample chamber of a Fluorolog-3 fluorometer for the PL measurements. The same fluorometer was used for PL measurements of PHOLEDs.

Electrically detected electron paramagnetic resonance (EDEPR) measurements were performed on a modified Varian E-9 EPR spectrometer operating in X-Band (9.1 GHz). A helium cryostat inside the EPR cavity allows for variable sample temperatures between 4 and 300 K. The EDEPR modification consists of a sample mount that permits electrical contacts to the sample OLED device inside the cavity. The OLED sample is cut to a 4 mm width and glued to an electrical connector (LEMO FFA.0S.304.CLAC42). Thin gold wires are attached to the anode and cathode contacts of the OLED device via silver paste and soldered to the terminals of the connector. A stainless steel tube serves as a conduit for wires inside the cryostat. The wires are attached to the OLED via a complementary connector. The OLED is positioned in the nodal plane of the microwave electric field. A low-noise constant-current source (Keithley 237) provides the operating current for the OLED device via a connector at the other end of the conduit. Because the relative changes in device voltage under resonant condition $\Delta V/V$ are smaller than 10^{-4}, we use the magnetic field modulation of the spectrometer combined with lock-in detection in order to improve signal-to-noise ratio. The modulation frequency, 35 Hz–10 kHz, is chosen to minimize noise while maintaining an adequate response time. A lock-in amplifier (Stanford Research Systems SR530) is connected in parallel to the OLED device and generates the demodulated signal.

III. RESULTS AND DISCUSSION

A. Material parameters

The materials are shown in Fig. 1, and relevant properties are listed in Table I. HOMO energies were obtained both as ionization potentials from UPS, when available, and also from electrochemical oxidation potentials when the oxidation was reversible. Data from irreversible oxidation waves are shown only when UPS data are unavailable. To facilitate comparisons, a constant of 4.45 eV was added to the oxidation potentials (see Sec. II). LUMO energies were obtained from electrochemical reduction potentials, shifted by the same 4.45 eV. HOMO/LUMO energies obtained from irreversible oxidation or reduction potentials represent upper or lower bounds, respectively, and are generally considered to be within 0.3 eV of the reversible value.[48] (However, in the relatively rare case where the irreversibility results from concerted redox and bond breakage, the discrepancy may be much larger than 0.3 eV.)

Our experimental triplet energies agree fairly well with literature values.[3,4,7,49,50] The differences are most likely traceable to variations in sample format and to our method of interpreting the spectra, which is intended to accommodate

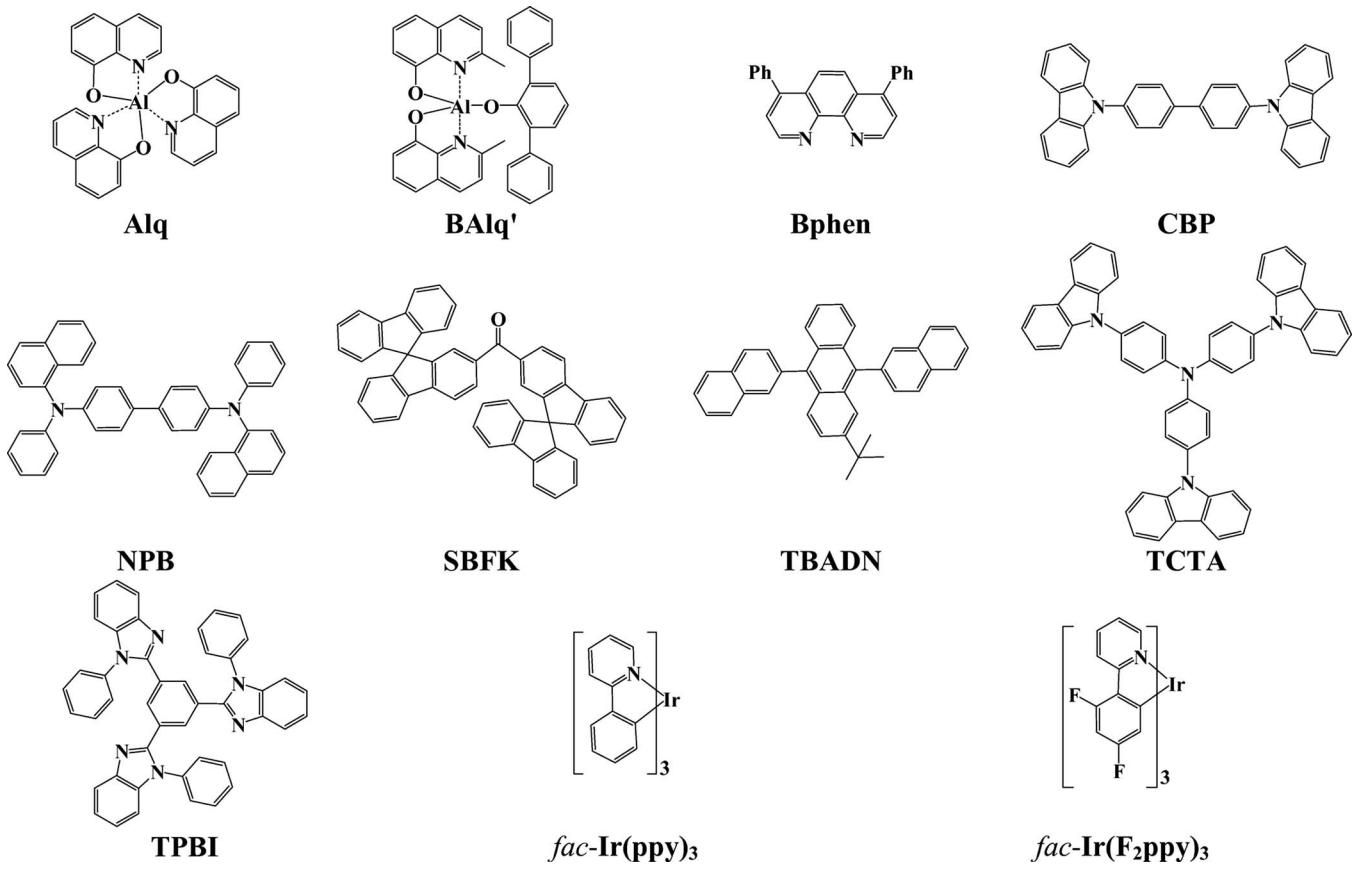

FIG. 1. Chemical structures of the principal materials.

unresolved vibrational structure. The largest deviation is for *N*,*N*′-di(naphthalen-1-yl)-*N*,*N*′-diphenylbenzidine (NPB), 2.41 versus 2.29 eV.[7] With two exceptions, the calculated (DFT) and experimental values agree adequately, and either method can be used for comparisons among materials. The exceptions are *bis*(9,9′-spirobifluoren-2-yl)ketone (SBFK) and Ir(F_2ppy)$_3$. The computational method has larger errors relative to experiment for fluorosubstituted iridium complexes, and it systematically underestimates the energies of carbonyl-based n-π^* triplet states.

The cohost mixtures investigated here are mixtures of TCTA with either TPBI or SBFK. Holes should reside preferentially on TCTA and electrons and triplets on TPBI or SBFK. Of the phosphorescent dopants, Ir(ppy)$_3$ should be a trap for holes and triplets, but not for electrons, whereas Ir(F_2ppy)$_3$ should be a trap for none of these species.

B. Device performance

The potential of a mixed-host structure to deliver high quantum efficiency and reduced drive voltage is illustrated by the following comparisons with more conventional PHOLEDs using a neat host.[51] The device structures are shown in Table II. 4,4′-*bis*(*N*-carbazolyl)-1,1′-biphenyl (CBP) is a representative neat host (devices A and C), and TPBI (64%) and TCTA (30%) were used as electron- and hole-transporting cohosts (devices B and D). The green phosphorescent dopant Ir(ppy)$_3$ was present at 6% in each case. BAlq′ and Alq were used as electron-transporting materials. Note that the ancillary ligand in BAlq′ differs from that in the related compound known as "blue Alq" (BAlq).[27] NPB was used for the hole-transport layer. TCTA was also used in devices C and D as an exciton- and/or electron-blocking layer (EBL).

Device performance is summarized in Fig. 2. Both mixed-host devices (B and D) are substantially more efficient at low current densities than the neat-host controls (A and C) and approximately the same at medium-to-high current densities. The use of the mixed host, however, decreases the drive voltages by as much as 2 V. For the more efficient mixed-host device (D), the EQE reaches ~20% at the lowest

TABLE II. Device structures for comparison of neat and mixed LEL hosts. Columns represent layers in order of deposition. Numbers are thicknesses in nm. LEL consists of 6% Ir(ppy)$_3$ in either CBP or TPBI+30% TCTA.

Device	ITO	CF_x	NPB	TCTA	Host+Ir(ppy)$_3$	BAlq′	Alq	LiF	Al
A	25	1	105		CBP, 35	10	40	0.5	100
B	25	1	105		TPBI+TCTA, 35	10	40	0.5	100
C	25	1	95	10	CBP, 35	10	40	0.5	100
D	25	1	95	10	TPBI+TCTA, 35	10	40	0.5	100

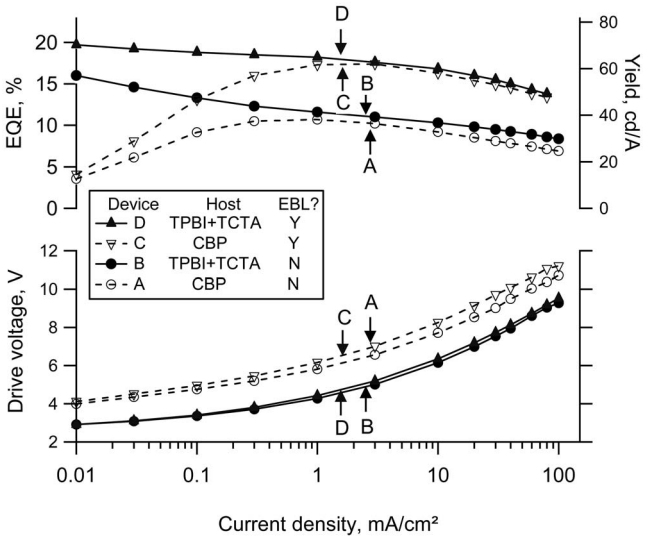

FIG. 2. EQE, luminous yield and drive voltage as functions of current density for green PHOLEDs with mixed-host TPBI+TCTA or neat-host CBP. Device structures are shown in Table II. Open and filled symbols are data points for neat-host and mixed-host devices. The arrows indicate 1000 cd/m^2 points. A single curve represents both EQE (left axis) and luminous yield (right axis) because the color is essentially constant. CIE coordinates are in the ranges (0.303−0.309, 0.310−0.311).

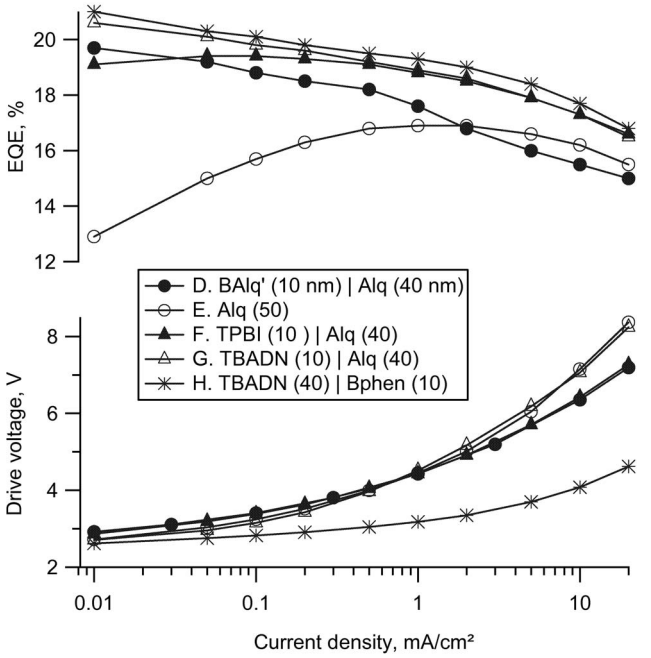

FIG. 3. Performance of devices with various ETLs (see legend). Organic layers: NPB(95 nm)|TCTA(10 nm)|TPBI+30%TCTA +6%$Ir(ppy)_3$(35 nm)|ETL. Anode and cathode are always ITO|CF_x and LiF|Al. CIE coordinates are all in the ranges (0.296−0.308, 0.625−0.634).

current density and exceeds ~14% throughout the entire range of currents. The points corresponding to 1000 cd/m^2 are indicated with arrows in Fig. 2. The power efficiencies at these points are 24 and 40 lm/W for the mixed-host devices (B and D) and about 30% lower for the neat-host controls (A and C). The main reason for the higher power efficiency of the mixed-host devices is their lower drive voltage. The use of TCTA as an EBL also improves the EQE and power efficiency at little cost in voltage. Similarly significant advantages in the performance of mixed-host versus neat-host devices were observed for blue PHOLEDs and will be discussed below.

The only difference between devices A (or C) and B (or D) is the use of the conventional neat host in one (A and C) and the mixed host in the other (B and D). The strikingly lower drive voltage can be attributed to more facile injection of charge carriers into the LEL as a consequence of its higher HOMO and lower LUMO levels, leading to a smaller potential-energy drop across the mixed-host LEL. The compatibility of these transport levels with an adequate triplet energy of the host is a consequence of the fact that the overall HOMO and LUMO reside on different molecules. Consider a hypothetical neat host with the same transport levels as the mixed host. They are closer than the HOMO and LUMO of CBP by ~0.9 eV. If the triplet level is shifted by the same 0.9 eV, this host material would have a triplet energy of 1.7 eV, far below that of the phosphorescent dopant. The device EQE would certainly be very poor. In contrast, the triplet level of the present mixed host is ~2.7 eV, and the devices using it are efficient.

In each of devices A−D, a substantial contribution to the remaining drive voltage is the potential drop across the ETLs, and the drive voltage can be further improved by reducing this contribution. This aspect is illustrated by devices and data reported in Fig. 3. The devices are identical to device D, except that the ETLs are varied. With one exception (50 nm Alq), the EQE curves are very similar, both in trend and in absolute magnitude. For all devices with a thick Alq layer adjacent to the cathode, the drive voltages are also very similar. The device with 2-(1,1-dimethylethyl)-9,10-di-2-naphthalenylanthracene (TBADN)|Bphen as the ETLs (device H), however, exhibits a much lower drive voltage. The improvement ranges from ≥1.2 V at 1 mA/cm^2 to ≥2.6 V at 20 mA/cm^2. Largely as a result of the reduced drive voltage, the power efficiency at 1000 cd/m^2 is 30%−70% higher than for the others (64 versus 37–48 lm/W). The reduced drive voltage is, at least in part, a consequence of a weaker electric field in the TBADN ETL (see below).[52]

It has become conventional to call the electron-transporting layer adjacent to the LEL a hole-blocking layer (HBL). This terminology connotes that the HOMO of this layer must be significantly deeper than the HOMO(s) of the hole-transporting component(s) of the LEL. It has further been assumed that the triplet state of this layer should lie well above those of the LEL materials. These assumptions have been questioned recently for devices with a neat CBP host material and a BAlq′ HBL.[27] According to Table I, each of the "HBL" materials is potentially hole blocking, but only TPBI has a sufficiently high triplet energy. TBADN has, by far, the lowest triplet energy of all, but devices with TBADN in the HBL are very efficient. Evidently, in the present device structure, the triplet energy of this layer is (or can be made) irrelevant, and one may select the HBL material on the basis of its electron injection and transport properties and operating stability without regard to its triplet energy. As will be discussed later, the emission zone in these devices usually does not extend to the LEL|HBL interface, so the relative

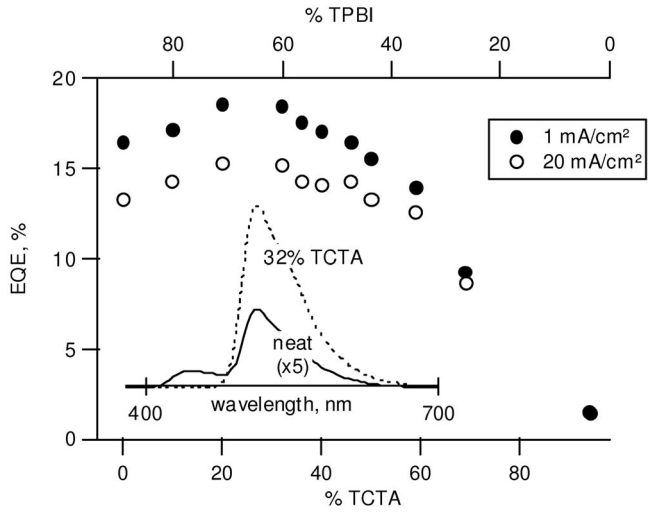

FIG. 4. Dependence of efficiency on composition of the mixed host. Organic layers: NPB(95 nm)|TCTA(10 nm)|TPBI+x%TCTA +6%Ir(ppy)$_3$(35 nm)|TBADN(40 nm)|Bphen(10 nm). The inset shows spectral radiance for devices with two host compositions at 20 mA/cm^2. Lower spectrum (neat TCTA host) is amplified 5×.

HOMO levels should also be irrelevant. For this reason, we abandon the identification as a (potential) HBL and refer to this layer simply as an ETL. An ETL adjacent to the cathode (e.g., Alq or Bphen) will be called either an ETL or an electron-injection layer (EIL). The two will collectively be called the ETLs.

An important advantage of the mixed-host architecture is that one can readily adjust the hole- and electron-transporting properties of the LEL by varying the proportions of the cohost materials. The effect of such variation is shown in Fig. 4. There is a broad optimum with respect to the efficiency around 30% TCTA, with almost no variation in the drive voltage (not shown) except for a modest increase with neat TCTA. The 1931 CIE coordinates are essentially constant (0.29, 0.63) except that the device with neat TCTA, which emits weakly overall, exhibits a significant blue (TBADN) component (see inset, Fig. 4).

Dopant concentration does not appear to be a critical variable for efficiency and voltage. From 1% to 6% Ir(ppy)$_3$, the EQE varies by 10%−15%, and it falls off gradually at higher concentrations. From 1% to 10% Ir(ppy)$_3$, the drive voltage at 20 mA/cm^2 varies by no more than 0.25 V and CIE (x,y) coordinates by no more than (0.03, 0.01). Undoped devices exhibit a weak, broad, blue exciplex emission (see Fig. 10), which disappears rapidly with increasing dopant concentration.

Blue or blue-green PHOLEDs place more stringent demands on the energy levels of the host, frequently resulting in limited efficiency and/or high drive voltage. The same device architecture—a mixed LEL host and an adjacent ETL that is chosen without regard to its triplet energy—can be used to make an efficient, low-voltage, blue-green PHOLED. As an example, PHOLEDs were made using the "sky-blue" dopant Ir(F$_2$ppy)$_3$. Device data are given in Table III. Device I uses neat TPBI as a single-component host, and device J uses the mixed host. The mixed-host device has more than double the EQE and a drive voltage that is reduced by >1 V. Replacing the ETLs of these devices by TBADN|Bphen (device K) further increases the EQE by as much as 40% and decreases the drive voltage by ≥0.5 V. The two design changes improve the power efficiency by a factor of 6 at 200 cd/m^2. (This luminance is representative of what is required for the blue component of a white pixel.) At equal current densities, the voltage improvement associated with the better ETL system is less than that for the analogous green OLEDs (devices H versus F, Fig. 3), in part because the ETLs are thinner. Subsequent PL measurements suggest that the LELs of the sky-blue devices contain a triplet-quenching impurity, which confounds the comparison of the EQEs. Nevertheless, it is clear that this device structure is capable of low drive voltages and high EQEs, perhaps even higher than those reported here.

Although the efficiency of our mixed-host PHOLEDs is superior to that with the neat-host CBP, their operational stability is inferior. A major factor is probably the well-known instability of TPBI in an OLED environment.[53] To illustrate, Table IV shows the effect of replacing TPBI in the LEL, and then in adjacent ETL, with an alternative material, SBFK or PADN. Replacing TPBI by a more stable material in the LEL improves the half-life (t_{50}) five- to tenfold. Replacing TPBI in the ETL also helps, but less dramatically. The greater sensitivity to LEL host composition most likely results from the greater variety of chemically reactive species in the LEL (holes, electrons, and excitons) than in the ETL. The choice

TABLE III. Performance of blue PHOLEDs containing TPBI neat host or TPBI+TCTA mixed host and different formulations of ETL and EIL. General device structure is ITO|CF$_x$|NPB(75 nm)|TCTA(10 nm)|host+8% Ir(F$_2$ppy)$_3$(35 nm)|ETL|EIL|LiF|Al. In columns 3 and 4, lower entry is layer thickness. Power efficiencies (PEs) are shown at 200 cd/m^2. All CIE coordinates are in the ranges (0.151−0.155, 0.321−0.326).

Device	Host	ETL Thickness (nm)	EIL	At 1 mA/cm^2 EQE (%)	At 1 mA/cm^2 Bias (V)	At 20 mA/cm^2 EQE (%)	At 20 mA/cm^2 Bias (V)	PE (lm/W)
	TPBI	TPBI	Alq	2.6	5.2	1.9	7.7	2.5
I		10	20					
	TPBI	TPBI	Alq	6.0	3.9	5.1	6.6	9.3
J	+TCTA	10	20					
	TPBI	TBADN	Bphen	8.4	3.4	5.5	6.0	15.1
K	+TCTA	20	10					

TABLE IV. Performance and half-life (t_{50}) of green PHOLEDs with various electron-transporting (ET) materials and dopants. LEL comprises mixed host, ET cohost +30% TCTA, and 6% dopant. Data are at 1000 cd/m^2 (1–2 mA/cm^2).

Device	ET Cohost	Dopant	ETL Thickness (nm)	EIL	EQE (%)	PE (lm/W)	CIE_x CIE_y	t_{50} (h)
F	TPBI	$Ir(ppy)_3$	TPBI	Alq	18.7	44.1	0.327	200
			10	40			0.631	
H	TPBI	$Ir(ppy)_3$	TBADN	Bphen	19.1	64.0	0.295	200
			40	10			0.634	
L	SBFK	$Ir(ppy)_3$	TPBI	Alq	15.1	34.1	0.323	1100
			10	40			0.621	
M	SBFK	$Ir(ppy)_3$	SBFK	Alq	15.5	29.6	0.354	2100
			10	40			0.603	
N	SBFK	$Ir(ppy)_3$	SBFK	Bphen	14.9	43.7	0.316	2000
			40	10			0.625	
O	SBFK	$Ir(ppy)_3$	PADN	Bphen	16.8	61.5	0.326	1800
			40	10			0.620	
P	TPBI	$Ir(5'phppy)_3$	TPBI	Alq	20.1	43.9	0.327	500
			10	40			0.631	
Q	SBFK	$Ir(5'phppy)_3$	TPBI	Alq	18.2	43.9	0.349	5300
			10	40			0.617	
R	SBFK	$Ir(5'phppy)_3$	SBFK	Alq	18.3	41.1	0.352	6500
			10	40			0.615	

of LEL dopant also matters, although to a lesser degree, as illustrated by the greater lifetime achieved when $Ir(ppy)_3$ was replaced by $Ir(5'phppy)_3$.

It was anticipated that a mixed host would lead to lifetime improvements relative to the individual components as neat hosts. In fact, in a limited number of comparisons, the half-lives with a mixed host were up to three times as long as those obtained when the electron-transporting cohost was used as a neat host instead (t_{50}'s evaluated at equal current densities, 1 mA/cm^2). (TCTA as a neat host would not be appropriate for this comparison because the device efficiency is very low.) It is not known why the lifetime improvements were so modest, but one possibility is that the recombination zone is still rather compact in the mixed-host devices (see below). Another less plausible explanation is that the loss of luminance is determined more by the number of chemical degradation products in the recombination (or luminescent) zone than by the concentration.

C. Location of the recombination zone

We turn now to issues of mechanism, beginning with the location of the recombination zone. We focus on devices with TBADN|Bphen ETLs because of their improved performance, but compare them briefly with devices containing TPBI|Alq ETLs to analyze the improvements. The latter are chosen as an example of mixed-host PHOLEDs with higher drive voltages and different conditions at the LEL|ETL interface. Except as noted, the LEL composition is TPBI:TCTA:$Ir(ppy)_3$, 64:30:6. We focus on the behavior at 20 mA/cm^2 to highlight the effects of device structure on drive voltage (Sec. III D). While the efficiencies are greater at lower current densities, the trends are similar.

The effect of varying the LEL thickness is illustrated in Fig. 5. Both the total device thickness and the distance from the EBL|LEL interface to the cathode are kept constant in order to minimize the confounding effect of varying optical interference (weak microcavity) effects. The EQE increases rapidly up to a thickness of 8 nm, then very gradually up to about 20 nm. As the LEL is made thicker, the location of the recombination zone probably shifts somewhat. So, Fig. 5 probably cannot be translated directly into a profile of the recombination zone within a thick LEL. Nevertheless, for LELs of ordinary thickness (~35 nm), it is reasonable to surmise from Fig. 5 that most of the recombination occurs within a zone about 10 nm thick, and that the remainder of the LEL acts mainly (although not entirely) as a unipolar

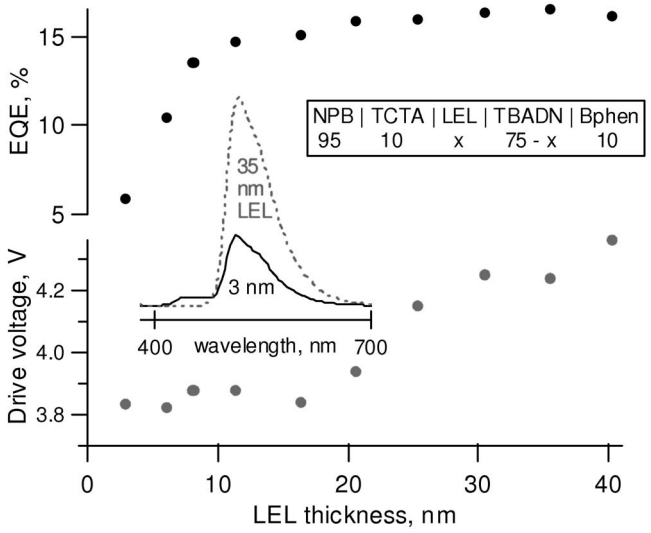

FIG. 5. EQE and drive voltage at 20 mA/cm^2 for a series of OLEDs with varying thickness of the LEL. The inset shows spectral radiance spectra for LELs 3 and 35 nm thick. Total device thickness is constant. Legend indicates thicknesses of organic layers in nm. LEL composition is 64:30:6 TPBI:TCTA:$Ir(ppy)_3$.

TABLE V. Device structures featuring a constant LEL thickness and a range of distances (x) between the EBL|LEL interface and the cathode. Devices S_x and T_x were fabricated in the same run. Device H is a standard device from a different run. Device names are in column 1. Numbers are layer thicknesses in nm. LEL is TPBI:TCTA:Ir(ppy)$_3$, 64:30:6. Anode is always ITO(25 nm)|CF_x(1 nm). Cathode is always LiF(0.5 nm)|Al(100 nm).

Device	NPB	TCTA	LEL	TPBI	TBADN	Bphen
S_x	200−x	10	35		x−45	10
H	95	10	35		40	10
T_x	200−x	10	2.3	20	x−32	10

charge-transport layer. Various pieces of evidence indicate that this recombination zone is located near the EBL|LEL interface. For one, because TBADN has a very low triplet energy (Table I), substantial recombination at the LEL|TBADN interface would make the devices inefficient because the triplets would devolve to TBADN.

A second view of the thickness dependence is provided in Fig. 6. Here only the thickness of the LEL varies, and the two ETL systems are compared. For both, the thinner LELs exhibit a relatively low efficiency, but more so with TBADN|Bphen as the ETL. Because the EBL|LEL interface is common to all of the devices, that low efficiency is most likely due to the proximity of the LEL|ETL interface. If so, for devices with a thick LEL, the much higher efficiency implies that the recombination zone is distant from the ETL, i.e., either somewhere in the middle or concentrated near the EBL|LEL interface.

For a thin LEL, there are several possible reasons why the efficiency is greater with TPBI as the adjacent ETL material than with TBADN. Triplets residing on Ir(ppy)$_3$ adjacent to the ETL should be quenched by TBADN (see below) but not by TPBI. Triplets carried by TPBI within the LEL may diffuse into the adjacent ETL. They may re-enter the LEL if the ETL material is TPBI, but not if it is TBADN. Holes carried by TCTA to the interface should not escape into TPBI; the lesser barrier presented by TBADN may allow some holes to escape. For the thickest LELs, the falloff in efficiency is most likely a consequence of optical interference effects that occur when the emission zone is poorly placed relative to the cathode.

The location of the recombination zone can be investigated in LELs of constant practical thickness if they are placed at such distance(s) from the cathode that the efficiency and spectrum are strongly affected by the location of the emitting molecules. A series of such devices (S) is described in Table V. A second series of devices (T), also described in Table V, features thin (nominally 2.3 nm) LELs and is used to generate the spectrum and relative outcoupling efficiency for precisely defined LEL-to-cathode distances. The location of the LEL is varied by changing the thicknesses of the TBADN ETL and the NPB HTL, keeping the total device thickness constant. These variations should not affect the internal dynamics (electric field profile, current and charge densities, recombination profile) of the LEL (see below). With the thin LELs, an adjacent hole-blocking ETL

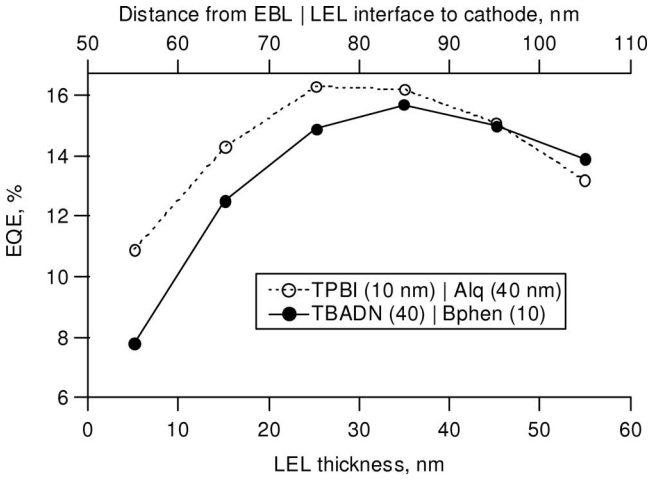

FIG. 6. EQE at 20 mA/cm^2 for OLEDs with varying thickness of the LEL (bottom axis) and varying distance of the EBL|LEL interface from the cathode (top axis). Organic layers: NPB(95 nm)|TCTA(10 nm)|LEL(x)|ETLS (see legend).

(TPBI) is incorporated to enhance the efficiency. Included in the comparison is a standard device with optimized layer thickness (H; cf. Table IV).

Figure 7 compiles the spectra for thick (solid curves, left stack) and thin LELs (all curves, right stack). Both the bandshape and the overall intensity (outcoupling efficiency) change markedly as the location of the LEL is varied in steps of 10 nm. Moreover, the bandshapes and relative intensities of devices with thick and thin LELs agree semiquantitatively if they are compared at equal distances (x) from the EBL|LEL interface to the cathode. It is clear that the emission zone and *a fortiori* the recombination zone are concentrated near that interface. The agreement becomes nearly perfect if the spectrum of a thick-LEL device at distance x (S_x,

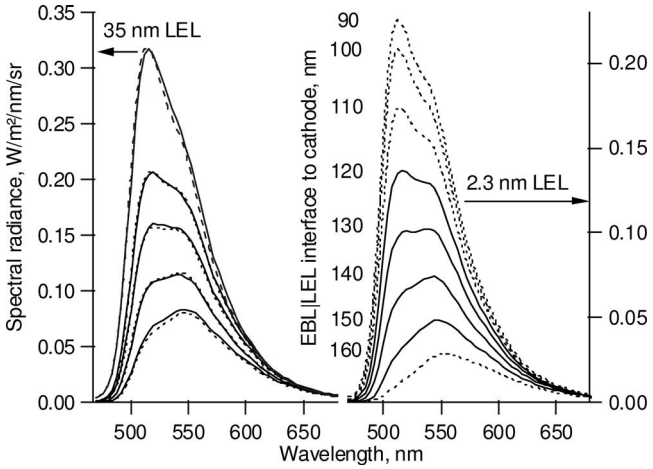

FIG. 7. EL spectra (20 mA/cm^2) parametric in spacing from LEL|EBL interface to the cathode. Spacing is indicated in center column; the numbers are aligned with the peaks of corresponding spectra in both stacks. Detailed structures are given in Table V. Left and right stacks and spectral radiance scales, for standard (35 nm) and thin (2.3 nm) LELs, are adjusted to compensate for the lesser efficiency of thin LELs. All curves for 2.3 nm LELs are experimental spectra; solid curves are selected for emphasis. Solid curves for 35 nm LEL are experimental spectra; dotted curves are two-component fits to linear combinations of thin-LEL spectra. The top left pair of curves is an exception: 85 nm spacing, single-component fit.

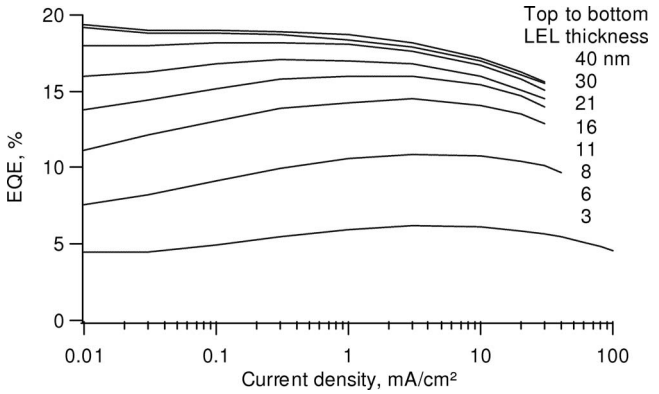

FIG. 8. EQE vs current density, parametric in thickness of the LEL (legend). Devices are the same as in Fig. 5.

Table V) is compared with a suitable linear combination of spectra of thin-LEL devices ($T_{x'}$) at distances $x'=x$ and $x-10$. That is, spectrum(S_x) $\approx c_1$ spectrum(T_x) $+c_2$ spectrum(T_{x-10}). A combination with $c_1=1$ and $c_2=0$ would be appropriate if all of the emission occurred at the interface and the thin and the thick LELs were equally efficient. The actual coefficients, $c_1=0.82$ and $c_2=0.55$, suggest that the emission zone of the thick LEL is spread over a substantial fraction of the 10 nm adjoining the TCTA|LEL, but not much further. The sum of the coefficients is larger than 1 because the thick LELs are somewhat more efficient than the thin (cf. Fig. 6). Figure 7 includes one more device (structure H) with a 35 nm LEL at the optimum distance (85 nm). Around that distance, the bandshape and intensity vary weakly, and a single reference spectrum (2.9 nm LEL, 85 nm from the cathode) suffices to reproduce the spectrum. The coefficient c_1 is close to the sum of the coefficients for the other devices, 1.28 versus 1.37. This agreement roughly confirms that we have properly accounted for the absolute intensities as well as the bandshapes of the other thick-LEL devices. The fits shown in Fig. 7 all include a 2 nm wavelength shift of undetermined origin.

This experiment probes the emission zone, which is wider than the recombination zone to whatever extent that triplets migrate before being captured by $Ir(ppy)_3$. Thus, the recombination zone appears to be concentrated well within ~10 nm from the EBL|LEL interface. This result is consistent with the tentative conclusion from the thickness dependence of the EQE. Even though the recombination zone is thin, it cannot be confined to the exact EBL|LEL interface because holes encounter no barrier there.

The above comparisons are all made at 20 mA/cm^2. The dependence of the efficiency on LEL thickness varies somewhat with current density. Equivalently, the dependence of the EQE on current density varies subtly with LEL thickness, as shown in Fig. 8. This effect appears to be connected with the use of TBADN|Bphen as the ETL and was not observed with TPBI|Alq. We have not attempted to analyze this phenomenon.

We return briefly to the cause of inefficiency with thin LELs. When TBADN is the adjacent ETL material, plausible explanations include escape of holes into the TBADN, recombination at the LEL|TBADN interface that produces mostly triplet-state TBADN, or recombination close to that interface where triplets are quenched by the TBADN. In fact, the devices used for Fig. 5 show a blue TBADN component of the emission that could arise from any of these processes (see inset, Fig. 5). It amounts to 7% of the EQE for the 2.3 nm LEL and falls approximately exponentially with increasing LEL thickness to at least 25 nm ($1/e$ distance of ≈4 nm), presumably signifying a decrease in the hole current reaching the LEL|ETL interface. As for quenching of triplets that are generated at or near the interface, PL measurements on the devices of Fig. 5 indicate that there is a "dead zone" at least 1.5 nm thick adjacent to the LEL|TBADN interface where $Ir(ppy)_3$, when excited directly, luminesces weakly if at all. When the adjacent ETL material is TPBI, on the other hand, triplets should not be quenched, and a large energetic barrier should also prevent holes from escaping (see Table I). Perhaps this is the reason why thin LELs are more efficient with TPBI|Alq as the ETLs than with TBADN|Bphen. Still, thin LELs adjacent to TPBI are less efficient than thick LELs. Perhaps this lesser efficiency is related to diffusion of triplets into the TPBI layer.

As illustrated in Fig. 4, the efficiency depends on LEL composition weakly up to about 40% TCTA, then falls rapidly at higher percentages. A likely explanation of the falloff, again, is hole current reaching the LEL|TBADN interface. The falloff coincides with the appearance of a blue TBADN component of the emission, detectable at 50% TCTA and prominent in the device with neat TCTA as the host (20% of the total emission at 1 mA/cm^2, 13% at 20 mA/cm^2). Another possible factor is a deterioration of triplet transport at low TPBI concentrations. As the cohost with the lower triplet energy, any migration of triplets occurs mostly via TPBI molecules. If migration is impeded, quenching and nonradiative decay to the ground state may compete with capture by $Ir(ppy)_3$.

D. Voltage budget

The dependence of the drive voltage on layer thickness is shown in Fig. 9. The data are offset vertically in order of increasing distance from the cathode. Ideally, to construct such a figure, the thickness would be varied for one layer at a time, while the other layers are maintained at thicknesses typical of optimized devices. The dependence on thickness of the EBL (TCTA) and of the main ETL (TBADN) was evaluated in this way. To investigate the LEL, its thickness was increased while that of the adjacent ETL (TBADN) was decreased, keeping the sum constant (lower panel, Fig. 5). Then, the independently measured dependence on TBADN thickness was used to recover the dependence on LEL thickness alone. When the two layers have similar thickness dependences, this procedure allows for a direct determination of the relatively small difference between them using devices fabricated in a single run. The 10 nm Bphen layer was assumed to be equivalent to 5 nm of TBADN. Previous experiments with the layer combination Bphen|LiF|Al indicate that an approximately 5 nm sublayer adjacent to the cathode is conductive enough that it does not contribute appreciably

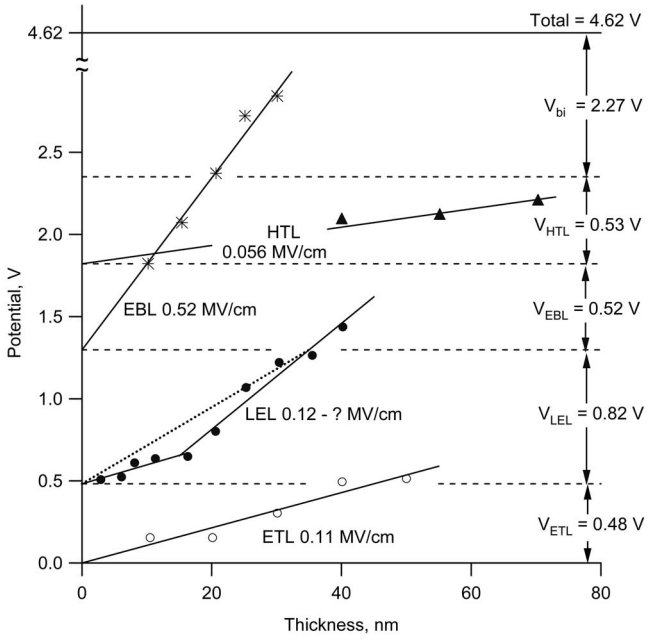

FIG. 9. Dependence of drive voltage (at 20 mA/cm^2) on thickness of the various layers. This representation provides insight into the voltage budget and the profile of the electrostatic potential inside the device. For each layer, data are shifted vertically in order of increasing distance from the cathode. The zero-thickness intercept for each layer (dashed line beneath the data) aligns with the potential of the preceding layer at a typical thickness (structure H, Table V). Data are labeled by layer and electric field strength. Contributions to the drive voltage are indicated at the right. For the HTL, EBL, and main ETL (TBADN), the slope of the linear fit is the electric field strength. For the LEL, the slope of the chord (dotted line) is the average field strength in a 35 nm LEL; the solid lines are a piecewise linear fit. The HTL data determining the linear fit include four additional points extending to 130 nm.

to the drive voltage. The contribution of the Bphen layer is probably very small anyway. The effect of varying the HTL (NPB) was assumed to be the same as for simple NPB|Alq devices (see below for justification).

To analyze the data, we assume (and will justify later) that the drive voltage V is the sum of an independent contribution from each layer plus the built-in potential V_{bi} associated with the work-function difference between the contacts.[31] Further, we assume that organic|organic interfaces, *per se*, do not contribute, i.e., that there are no internal dipole layers. As we vary the thickness of layer j, namely d_j, the resulting variation in the drive voltage $V(d_j)$ reflects the variation in the potential drop across that layer. The zero-thickness limit is denoted $V(0)$. Thus, $V(d_j)-V(0)$ represents the potential drop across layer j as a function of its thickness, while $V(0)$ for layer j represents the sum of all other contributions to the drive voltage. One can read the potential difference across each layer, for whatever thickness, directly from Fig. 9.

Each horizontal line in Fig. 9 is a baseline for one layer. The data for that layer are shifted vertically so that its $V(0)$ is on the baseline. The baseline for layer $j+1$ is drawn through the data for the previous layer (j) at a level corresponding to a typical thickness of layer j. Thus, the distance between the baselines for layers j and $j+1$ indicates the portion of the drive voltage associated with layer j for that thickness.

The sum of the contributions of individual layers, represented by the top line, is 2.34 V. It should represent the total contribution of the organic layers to the overall drive voltage. The built-in voltage, measured independently, is 2.27 V. Combining these contributions gives a "predicted" drive voltage of 4.62 V. The actual drive voltage is 4.6 ± 0.1 V (five devices from separate fabrication runs). This agreement is one confirmation of the analysis. A more detailed justification is presented in the next section.

Except for the thin, semiconducting portion of the Bphen layer, each layer of the device makes a similar contribution to the drive voltage. The analysis offers a prospectus for further voltage improvements. The contribution of the ETL (0.5 V) might be reduced by as much as 0.3–0.4 V by using a much thinner layer of TBADN together with a thicker semiconducting ETL, perhaps codeposited Bphen:Li. The contribution of the HTL (0.5 V) can nearly be eliminated by *p*-type doping[54] of the NPB (except near the LEL). Alternatively, a thinner HTL can be used together with thicker ITO to reoptimize the optical microcavity effects. The EBL is already thin, and probably cannot be made much thinner without changing the EL efficiency. Making the LEL thinner would entail a tradeoff between lower drive voltage and lower EQE. The proper tradeoff would depend on the intended application. Making the "easy" changes to the HTL and ETL should bring the drive voltage (at the present 20 mA/cm^2) below 4.0 V. It should not affect the boundary conditions governing the dynamics and the performance of the LEL.

As discussed above, devices with TBADN|Bphen as the ETL have much lower drive voltages than those with Alq as the main ETL, and the difference ($\geq$1.3 V) was tentatively ascribed to the weaker electric field in the ETL. Large voltage reductions for combinations of Bphen with a similar anthracene derivative have been reported before.[52] An analysis similar to that in Fig. 9 was carried through for a representative set of higher-voltage devices with TPBI|Alq as ETLs of various thicknesses. For a typical device with 10 nm TPBI and 40 nm Alq (F, Fig. 3), the ETL contribution to the drive voltage is indeed higher, by ~2.3 V, than with TBADN|Bphen (structure *H*). However, the contribution of the LEL is also much higher, namely 2.2 V, as compared to 0.8 V with TBADN (40 nm)|Bphen(10 nm). That is, the voltage improvement with TBADN|Bphen arises partially from its own improved injection and transport properties and partially from its influence on electric field in the LEL. There is also a modest compensating difference in the built-in voltage, which is 0.3 lower with TBPI|Alq. It is remarkable that the different fields in the two ETLs barely affect the EQE behavior of the LEL (Fig. 3).

E. Electric field profile and charge distribution

1. Analysis

For each single-carrier layer, the associated potential drop varies linearly with the thickness (Fig. 9). The natural inference is that the electric field is constant through each of these layers, and the potential drop is the product of the field strength and the layer thickness. The electric field strengths,

obtained from the linear fits, are also noted in the labels in Fig. 9. A constant field through a layer implies that space charge there is negligible. A small difference of the field in neighboring layers could represent a small difference of the dielectric constant or a systematic error of the layer thicknesses, but a large difference implies an accumulation of charge at the interface between the layers. In Fig. 9, an increase (or decrease) in the slope from one layer to the layer above it implies a negative (or positive) charge at the interface. Assuming a relative dielectric constant of 3.5 for both layers (the value for NPB and Alq[55,56]), there is an accumulation of $+140\ \mathrm{nC/cm^2}$ $(9\times10^{11}\ \mathrm{holes/cm^2})$ at the NPB|TCTA interface. Thus, there appears to be an injection barrier at this interface, consistent with the electrochemical data in Table I.

The potential drop across the LEL varies nonlinearly with layer thickness. Either the field in the LEL is not uniform or it is uniform but its strength varies with layer thickness. Further, the LEL is bipolar, and any charge distribution within it may vary with LEL thickness. Therefore, any interpretation of LEL contributions in Fig. 9 must be more tentative than for the single-carrier layers. It will help to note three facts. (1) The potential drop across any layer is identically the product of the thickness and the *average* field in the layer, regardless of the details of the charge distribution and regardless of how they might vary with varying thickness. One can evaluate the average field in a LEL of any particular thickness by drawing a line from the corresponding data point to the zero-thickness limit; the average field strength is given by the slope of that line (chord to the curve, dotted line, Fig. 9). (2) Also independently of the details of the charge distribution, the ETL must be shielded from the higher field in the EBL by an accumulation of negative charge somewhere between those two layers. This charge must add up to $-130\ \mathrm{nC/cm^2}$ $(8\times10^{11}\ \mathrm{electrons/cm^2})$. (3) The EL data in Sec. III C indicate that the recombination zone in thick LELs is concentrated near the EBL|LEL interface.

For LELs thinner than about 15 nm, the voltage plot is linear and roughly parallel to that for the TBADN layer. Therefore, the average field in a thin LEL is about the same as in the TBADN $(\sim1.1\times10^5\ \mathrm{V/cm})$ and much smaller than the field in the EBL $(5\times10^5\ \mathrm{V/cm})$. A reasonable inference is that the field in most of the LEL is uniform and approximately equal to that in the ETL. If so, the total of $-130\ \mathrm{nC/cm^2}$ resides at the EBL|LEL interface or nearby. The rest of the LEL, including the LEL|ETL interface, is approximately neutral.

For LELs thicker than about 15 nm, the voltage plot turns upward. Now a portion of the nominal LEL adjoining the ETL functions largely as an auxiliary electron-transporting sublayer. If we assume that the voltage contribution of the recombination zone is now constant, the slope of the voltage plot indicates the field strength $(\sim3\times10^5\ \mathrm{V/cm})$ in that mostly electron-transporting sublayer. The stronger field in the EBL implies that part of the net $-130\ \mathrm{nC/cm^2}$ resides in the recombination zone or at the EBL|LEL interface. The weaker field in the adjacent TBADN layer implies that part of the net $-130\ \mathrm{nC/cm^2}$ also resides at the LEL|ETL interface. The interfacial negative charge suggests a barrier to injection from TBADN into TPBI. Drive-voltage data on electrons-only devices with a TPBI|TBADN interface also point to such a barrier. The estimated LUMO levels (Table I) also suggest it, but the difference is too small for a reliable prediction.

The picture is not yet complete. The average field within the LEL (slope of the chord in Fig. 9) is smaller than the field in the mostly electron-transporting sublayer (slope of the high-field data). Apparently, the field in the bipolar region (in or near the recombination zone) is weaker than in the rest of the LEL. If so, there is negative net charge at or very near the EBL|LEL interface, shielding the recombination zone from the higher field in the EBL, and there is a positive net charge deeper inside the recombination zone, supporting the stronger field in the mostly electron-transporting sublayer. Positive charge density in the recombination zone would not be surprising, as there is no barrier to injection of holes from the EBL.

As mentioned earlier, simple alterations of the HTL and ETL should reduce the drive voltage substantially without affecting the performance of the LEL. The remainder would consist mostly of the built-in potential and the contributions of the EBL and the LEL. According to the present analysis, the latter contributions are both determined largely by barriers to carrier injection.

According to the above interpretation of the voltage plot for the LEL, the upturn provides an alternative measure, ~15 nm, of the width of the recombination zone. The zone presumably has no sharp boundary inside the LEL, and different measures should generally yield different widths. The present ~15 nm is somewhat greater than the estimates based on the dependence of EQE on layer thickness and location (Sec. III C).

2. Justification of the analysis

The detailed hypotheses about the field and charge density in the LEL must remain tentative. We return now to justify the remainder of the analysis of the voltage budget and the profiles of field and charge density. The critical assumption is that each layer makes an independent contribution to the total potential drop and drive voltage. The additivity of the contributions is obvious, but their independence is less so. From the outset, it is encouraging that this assumption permits the drive voltage to be dissected and reassembled correctly. This result may also be taken as support for our further assumption that there are no dipole layers at the organic|organic interfaces.

The electric field at the anodic contact (ITO|CF_x|NPB) is determined by the current density and the injection properties of the contact (current density versus field strength), provided that the potential drop across the layer is large enough that transport is dominated by drift rather than diffusion. The field profile in the HTL is determined by the field at the anodic contact, the current density, and the transport properties of NPB. Thus, the contribution of the HTL to the drive voltage should be independent of the structure of the rest of the device. This is the basis for using simplified NPB|Alq reference devices to evaluate the HTL contribu-

tion. Consistent with this argument, we have found that the voltage plot for the NPB|Alq devices is indistinguishable from that of holes-only devices with the structure ITO|CF_x|NPB|Al. Given a plot of drive voltage versus thickness, $V(d_{HTL})$, the slope is necessarily equal to the field strength in the HTL at distance d_{HTL} from the anode in a layer of this thickness or any greater. The linear dependence of the drive voltage on HTL thickness indicates that the field is uniform over the range of interest. Thus, the field strength at the HTL|EBL interface is also independent of the thickness of the HTL. That boundary condition, the injection properties of the NPB|TCTA contact, and the transport properties of TCTA, together with the current density, determine the electric field profile in the EBL and its contribution to the drive voltage. Again, this contribution should be independent of the structure of the rest of the device, but only because the field in the HTL is essentially constant. Consistent with this argument, the electric field strength in the EBL (TCTA) is essentially the same, $(5.1–5.3)\times10^5$ V/cm (three experiments) regardless of whether the ETL is TBADN|Bphen or TPBI|Alq.

With the possible exception of devices with very thin LELs, the ETLs are also unipolar. The linear dependence on TBADN thickness again implies a uniform electric field. As with the EBL, the field strength in the TBADN ETL is essentially the same, whether the TBADN is directly adjacent to the LEL (1.07×10^5 V/cm, Fig. 9) or separated from the LEL by a 20 nm layer of TPBI (1.09×10^5 V/cm, device series T in Table V; data not shown). Finally, the boundary conditions presented to the LEL—the field strength and (unipolar) current density on both sides—are independent of the thicknesses of the other layers. Consequently, the internal dynamics of the LEL and the resulting electric field profile and potential drop must be likewise independent. This conclusion also underlies the analysis of the EL spectra in Fig. 7, which assumes that the profile of the recombination zone is independent of the thickness of the HTL and ETL. However, the *composition* of the other layers does matter, as indicated by the much larger average field in the LEL when the ETL is TPBI|Alq rather than TBADN|Bphen.

In this context, also note that a zero-thickness limit [$V(0)$, above] is not necessarily the same as the voltage in the actual absence of a layer. For example, removing an EBL changes the boundary conditions for the LEL, whereas the zero-thickness limit is intended to leave those conditions intact. It is presumably for this reason that inserting or removing the EBL often affects the drive voltage less than might be expected (see Fig. 2).

The LEL data in Fig. 9 actually represent total drive voltages, and we have assumed that only the contribution of the LEL varies. For a sufficiently thin LEL, however, some hole current necessarily reaches the adjacent ETL. If any is injected and conducted within the ETL, the voltage contribution of the ETL will actually depend somewhat on the thickness of the LEL. As the LEL is made thicker, the hole current reaching the TBADN layer decreases, the hole current inside the TBADN should also decrease, and the voltage contribution of the TBADN layer should increase. Thus, the degree to which the drive voltage increases may somewhat overestimate the contribution of the LEL alone. To the extent that this effect occurs at all, the EQE data in Fig. 5 suggest that it occurs mostly for LELs between 0 and 7.5 nm thick. The total variation in this range is ~0.1 V, so, apparently any confounding effect of hole current in the ETL introduces not more than ~0.1 V uncertainty in our estimate of the voltage contribution of the LEL. A plot of the actual LEL contribution should be parallel to the plot in Fig. 9 for thicknesses of ≥7.5 nm and shifted downward uniformly by not more than ~0.1 V. In fact, experiments that varied the thickness of TBADN for thin and thick LELs (3 and 34 nm) showed no detectable difference in field strength.

It is worth making explicit the meaning of the electric field discussed above. It is consistent with current OLED terminology; but, in textbook terms,[57] it is neither the microscopic field nor the macroscopic field in the layer. Rather, it is a two-dimensional average of the microscopic field over a plane parallel to the device plane at a given distance from the substrate. (The macroscopic field is conventionally defined as a weighted average over a small, but not infinitely small spherical region.) Over this plane, the microscopic field may vary substantially because of the discrete location of the charge carriers and the significant separation between them. The average field discussed above in the context of the LEL is a further average over the complete thickness of the layer. Or, equivalently, it is a three-dimensional average of the microscopic field over the volume of the layer.

F. Undoped devices

According to the LUMO levels in Table I, the electron carrier involved in recombination is almost certainly the radical anion of TPBI ($TPBI^-$). While $Ir(ppy)_3$ has a shallower HOMO than TCTA, it is also relatively dilute, and the dominant cationic species involved in recombination might be either $Ir(ppy)_3^+$ or of $TCTA^+$. The very mild effect of doping on the drive voltage, mentioned above, is a hint that $Ir(ppy)_3^+$ plays a limited role in transport and/or trapping and, therefore, recombination. Because recombination between the host species may be important to the operation of doped devices, we have examined the EL behavior of devices where only those species are present in the LEL. Electron paramagnetic resonance studies of the same devices are reported in the next section.

As mentioned above, the emission of undoped devices is weak, broad, and blue, very similar to the spectrum labeled "40 nm" in Fig. 10 (below). It was identified as a TPBI/TCTA exciplex by examining the PL spectra of TCTA, TPBI, and a 70% TPBI:30% TCTA mixture as 100 nm films deposited on ITO|CF_x. Each was excited at 330 nm. TPBI and TCTA fluoresce with maxima at about 410 and 388 nm, respectively. The spectrum of TPBI/TCTA mixture is relatively broad, and it peaks at 440 nm. The redshift and the breadth are typical of an exciplex. These samples had no Al cathode, so optical microcavity effects are minor. For instance, the emission maxima of 100 and 150 nm films of the TCTA/TPBI mixture differ by only 4 nm. Microcavity effects in complete OLEDs are much more significant. Depending on the layer thicknesses, EL peak positions from 445 to 464 nm

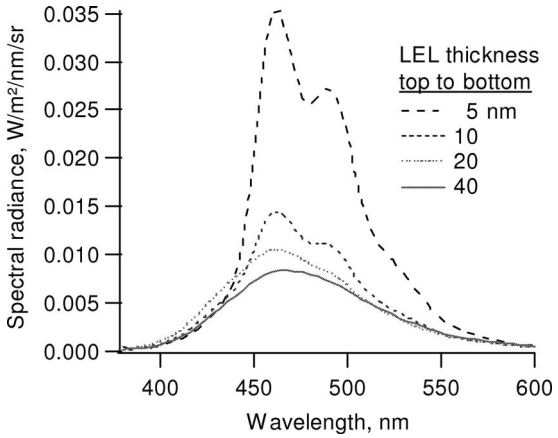

FIG. 10. EL spectra of devices with undoped mixed-host LELs of different thicknesses and an ETL doped with TBP as a probe (U1–U4, Table VI) at 20 mA/cm^2. Total device thickness and distance from the LEL|ETL interface to the cathode are constant. The top spectrum, with peaks at 463 and 490 nm, is typical of TBP. The bottom, nearly structureless spectrum is similar to that of the TCTA/TPBI exciplex.

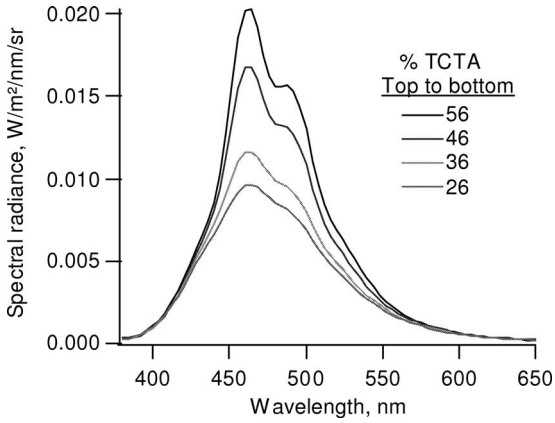

FIG. 11. EL spectra of devices having undoped LELs (20 nm) with different cohost ratios, and an ETL doped with TBP as a probe (V1–V4, Table VI) at 20 mA/cm^2.

were observed. The shifts, relative to the PL of the bare 100 nm film, are qualitatively reproduced by an optical model.[58,59]

To investigate the hole current potentially reaching the TBADN layer, we doped 20 nm of the ETL (TBADN) adjoining the LEL with a fluorescent blue emitter, TBP. Although the doped ETL can emit, we will reserve the term LEL for the mixed-host layer. The effect of LEL thickness and composition was explored using devices U1–U4 described in Table VI. Figure 10 shows how the EL spectra depend on the thickness of an LEL containing 30% TCTA. The emission with the thinnest LEL (5 nm) is dominated by TBP,[60] that with the thickest LEL (40 nm) is dominated by the host exciplex, and the intermediate thicknesses grade from one to the other. The most straightforward interpretation is that rather little hole current penetrates to 20 nm into the LEL.

The effect of varying the percentage of TCTA in the LEL (devices V1–V4, Table VI) is shown in Fig. 11. It appears, unsurprisingly, that higher TCTA concentrations result in an increased ability of holes to pass through 20 nm of the LEL without recombining. With regard to the limited range of hole transport, the undoped devices appear to behave similarly to the PHOLEDs described above. It is difficult to make the conclusions quantitative because of the unknown contribution of energy transport and/or transfer.

G. Triplet-state electron paramagnetic resonance

The operation of mixed-host PHOLEDs at low temperature was investigated using EDEPR spectroscopy. This technique has been applied previously to study the doublet species in OLEDs, i.e., the charge-carrying radical ions.[61,62] Here we apply it to the triplet states, whose spectra are typically more readily dissected into contributions of individual species. The best spectra are obtained at cryogenic temperatures, whereas the device physics at room temperature is of primary interest. To examine the potential of the technique, we have investigated the extent to which the device behavior inferred at low temperature mimics or contrasts with that at room temperature. Most experiments were conducted at 20 K, but it is occasionally possible to obtain useful spectroscopic data as high as 200 K (see Fig. 16, below).

The EDEPR experiment is similar to conventional EPR, but resonances are detected electrically. A device is driven at constant current, and a resonance is detected by a small increase or decrease in the drive voltage ($\leq$ a few millivolts). The magnetic field is modulated at 1−10 kHz, and the resulting modulation of the drive voltage is recorded. Reference triplet-state spectra of the individual materials were obtained via conventional EPR spectroscopy of photoexcited frozen solutions. The spectra corresponding to spin-allowed transitions ($\Delta m_S=1$) are usually structured and characteristic of the various species. The spectra corresponding to formally spin-forbidden transitions ($\Delta m_S=2$, half-field lines) are usually featureless but may occur at characteristic locations in

TABLE VI. Structures (organic layers) of devices featuring undoped LELs and TBP as a fluorescent probe in the ETL. Entries in columns 2, 3, and 5–7 are layer thicknesses in nm.

Device	NPB	TCTA	TPBI+TCTA	TBADN+1% TBP	TBADN	Bphen
			30% TCTA	20	20	10
U1–U4	125−x	10	x=5, 10, 20, 40 nm			
			26, 36, 46, 56 %TCTA	20	20	10
V1–V12	110	10	5, 10, 20 nm			
V3	110	10	36% TCTA, 20 nm	20	20	10
V7	120	10	36% TCTA, 10 nm	20	20	10
V11	125	10	36% TCTA, 5 nm	20	20	10

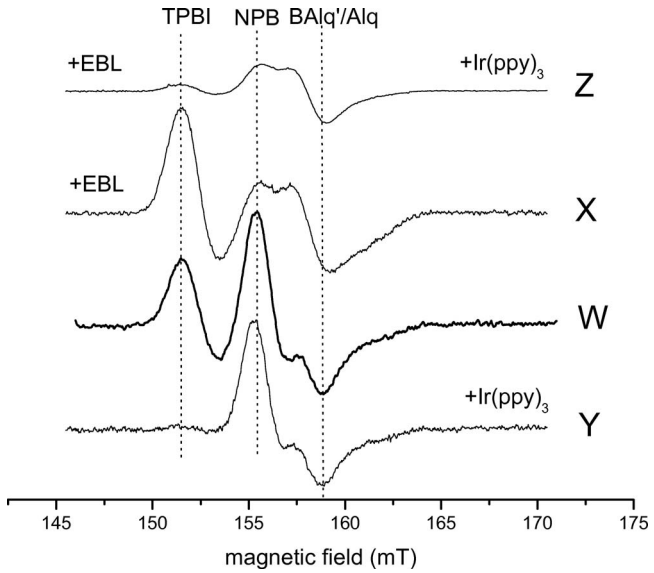

FIG. 12. EDEPR of model PHOLEDs at 20 K and 6 mA/cm^2 in the $\Delta m_S = 2$ region of the spectra. Organic layers: NPB|EBL (or none)|LEL|BAlq′|Alq (devices W–Z, Table VII). Trace annotations indicate the devices with dopant ($Ir(ppy)_3$) and/or an EBL (TCTA). The order of presentation is chosen to facilitate comparison of devices with or without these features. Peak labels identify (derivative) peaks that are characteristic of the various components. The spectra of Alq and BAlq′ are indistinguishable in this region of the spectrum. Under a resonance condition, the drive voltage at constant current decreases by about $\Delta V/V = 10^{-5}$.

the spectrum (g-values). In many cases the difference in location is large enough to resolve different triplet species. This fact affords a simple way to observe changes in triplet signal intensities when the structure and/or composition of the device is varied. EPR, in general, is sensitive to triplet states of organic molecules, but not of the Ir-complex dopants because of their very large zero-field splittings (⩾ the Zeeman splitting) and short excited-state lifetimes (leading to low steady-state concentrations). There are at least two ways that resonance—altering the population of triplets in the three possible spin states—can affect the drive voltage. If a triplet encounters a trapped charge carrier, the triplet may be annihilated and its energy may be spent to detrap the carrier. A similar process could "boost" a carrier across an energy barrier. The probability of these processes depends on the orientation of the spins of both species, so altering the populations of the spin states alters the rates of these transport-enhancing processes. Because of the complicated linkage between the spin resonance and its eventual effect on the drive voltage, the magnitudes of signals from different species are not proportional to their relative populations. For this reason, we focus on trends associated with variations in device structure or composition.

Figure 12 shows EDEPR spectra of operating devices (~6 mA/cm^2 at ~31 V) with BAlq′|Alq as the ETLs, with or without an EBL (TCTA), and with or without $Ir(ppy)_3$ as a phosphorescent dopant. The device structures are shown in Table VII. In undoped devices without the EBL, triplets from the HTL (^{3}NPB) and the ETL (either ^{3}BAlq′ or ^{3}Alq) as well as triplets localized on the TPBI cohost are observed (trace W). The appearance of TPBI triplets is evidence of bulk recombination. Recombination at either boundary would presumably produce mostly ^{3}NPB or ^{3}BAlq′, as both have a lower energy than ^{3}TPBI. The ^{3}NPB and ^{3}BAlq′ that are observed could be generated at the interfaces or generated within the LEL and migrate out. The appearance of triplets of TBPI, but not of TCTA, is consistent with their lower energy. Insertion of TCTA as an EBL between NPB and the undoped LEL increases the ^{3}TPBI signal and reduces the ^{3}NPB signal (trace X). This effect is consistent with the electron- and triplet-blocking character of the EBL. Doping of $Ir(ppy)_3$ into the mixed LEL in the absence (trace Y) or presence (trace Z) of the EBL nearly eliminates the ^{3}TPBI signal, but does not affect the ^{3}NPB or ^{3}BAlq′ signal. The effect of the EBL is still visible as a reduction of the ^{3}NPB signal in device Z as compared to device Y. Electron-hole recombination presumably occurs between the anion radicals of TPBI ($TPBI^{-}$) and the cation radicals $TCTA^{\cdot+}$, $Ir(ppy)_3^{\cdot+}$, and/or $NPB^{\cdot+}$ (at a HTL|LEL interface), initially producing ^{3}TPBI, $^3Ir(ppy)_3$, or ^{3}NPB. The effect of the $Ir(ppy)_3$ could represent either capture of triplets (energy transfer) from the TPBI cohost or a change in the cationic recombination partner from $TCTA^{\cdot+}$ to $Ir(ppy)_3^{\cdot+}$. The fact that the EBL does not entirely eliminate the ^{3}NPB signal suggests some leakage of either triplets or electrons through it. The EQEs for the two doped devices (room temperature, 20 mA/cm^2) are 9.6% without EBL and 16.2% with EBL. The increased ^{3}TPBI signal that we observe upon addition of the EBL in the undoped devices (X and W) is paralleled in an increase in device efficiency in the $Ir(ppy)_3$-doped devices (Z and Y).

TABLE VII. Structures (organic layers) of devices used for Fig. 12. Numbers are layer thicknesses in nm. The LEL contains 30% TCTA and 0% or 6% $Ir(ppy)_3$.

Device	NPB	TCTA	LEL	BAlq′	Alq
W	105		TPBI+TCTA, 35	10	40
X	95	10	TPBI+TCTA, 35	10	40
Y	105		TPBI+TCTA+$Ir(ppy)_3$, 35	10	40
Z	95	10	TPBI+TCTA+$Ir(ppy)_3$, 35	10	40

The EDEPR (~6 mA/cm^2 at ~25 V) of mixed-host devices with a TBADN|Bphen ETL is illustrated in Fig. 13. The device structures are summarized in Table VIII. Note that the operating voltage of these devices at 20 K is lower than that of the corresponding set with BAlq′|Alq as ETL. A device with no EBL and no dopant (trace AA) shows signals from ^{3}TPBI and ^{3}NPB, but none from ^{3}TBADN. Again, the ^{3}TPBI signal indicates that substantial recombination occurs within the (undoped) LEL. The absence of a ^{3}TBADN signal may mean that few triplets are generated in or near the ETL or that little charge is available to be mobilized by interaction

TABLE VIII. Structures (organic layers) of devices used for Fig. 13. Numbers are layer thicknesses in nm. The LEL contains 30% TCTA and 0% or 6% $Ir(ppy)_3$.

Device	NPB	TCTA	LEL	TBADN	Bphen
AA	105		TPBI+TCTA, 35	40	10
AB	95	10	TPBI+TCTA, 35	40	10
AC	95	10	TPBI+TCTA+$Ir(ppy)_3$, 35	10	40

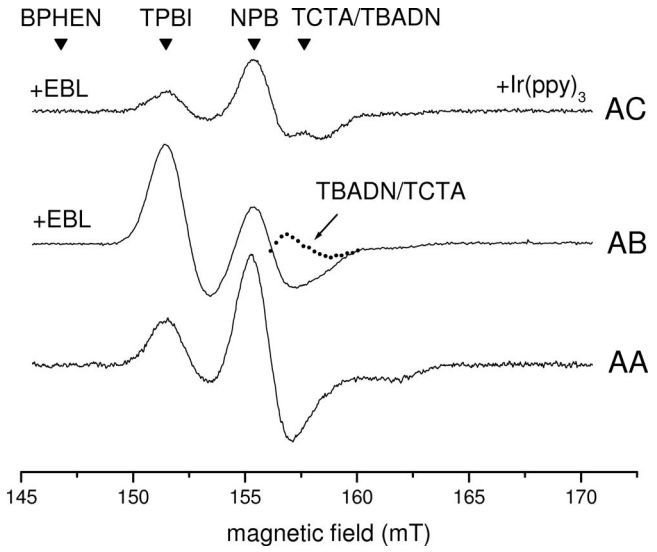

FIG. 13. EDEPR of model PHOLEDS at 20 K and 6 mA/cm^2. Organic layers: NPB|TCTA|LEL|TBADN|Bphen (devices AA−AC, Table VIII). Arrowheads indicate locations of (derivative) peaks characteristic of the components. In the high-field region, the different bandshapes of devices AA and AB indicate the presence of an additional component. Shown superimposed as the dotted curve, it could represent either TBADN or TCTA; their spectra are similar. Full-field spectra identify it as TBADN. No ^{3}Bphen signal is detected.

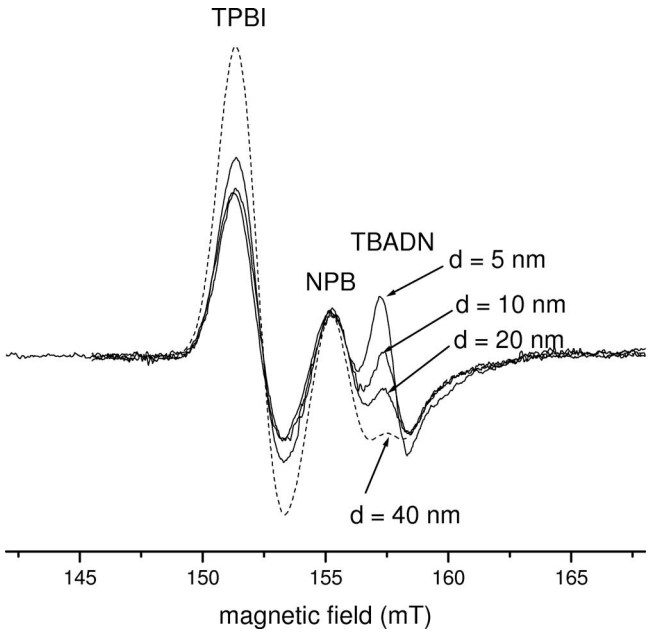

FIG. 14. EDEPR of OLEDs with undoped LELs of various thicknesses (d), adjacent to an ETL of TBADN:TBP. The organic layers are NPB|TCTA|TCTA+TPBI|TBADN:TBP|TBADN|Bphen (Table VI, devices U1−U4).

with triplets there. This observation is in contrast to the previous device set, with BAlq′|Alq as the ETL, where triplets in the ETL were readily observed. The difference may indicate that the choice of ETL has an influence on the profile of the recombination zone in otherwise identical devices, i.e., that the TBADN|Bphen ETLs lead to a recombination zone that is displaced further toward the HTL side of the LEL. Perhaps for the same reason, we have observed that the EQE at room temperature rises somewhat more slowly with increasing LEL thickness if BAlq′|Alq is the ETL rather than TBADN|Bphen. Insertion of a TCTA EBL (trace AB) again reduces the ^{3}NPB signal and increases that of ^{3}TPBI. The nominal ^{3}NPB peak is broader than in trace AA, indicating the presence of an additional, underlying peak. The entire spectrum, including the spectral range in question, can be synthesized by adding one more component. The spectral shape and position of that component (dotted curve in Fig. 13) point to either ^{3}TBADN or ^{3}TCTA; it is difficult to distinguish between their spectra in this range of magnetic field strength. Nevertheless, ^{3}TBADN is more probable because ^{3}TCTA should be quenched by any other material in the device. We will refer to it as ^{3}TBADN, although the proof will be offered later. Thus, the introduction of the EBL in this device structure has the additional effect of increasing either the recombination rate or the population of trapped charge near the ETL. Adding Ir(ppy)$_3$ to the LEL (trace AC) again suppresses the ^{3}TPBI signal significantly while there is not much change in the residual ^{3}NPB and ^{3}TBADN signals.

The effect of varying the thickness of the LEL in devices with the EBL but without the phosphorescent dopant was explored further using the same devices as were studied by EL at room temperature (devices U1–U4, Table VI). The EDEPR spectra (Fig. 14) again show contributions of ^{3}NPB, ^{3}TPBI, and either ^{3}TBADN or ^{3}TCTA. With the thinnest LEL (5 nm), the signal attributed to either ^{3}TBADN or ^{3}TCTA is large enough that corresponding features in the region of the spin-allowed transitions can be resolved. By comparison with reference spectra it can be positively identified as ^{3}TBADN. Comparison of the spectra in Fig. 14 shows that the largest effect of increasing the LEL thickness is a rapid decrease in the ^{3}TBADN signal. Going from a LEL thickness of 5 nm to 20 nm, the signal decreases by 55%, whereas those from ^{3}TPBI and ^{3}NPB increase by about 20%. The EDEPR spectrum for the thickest LEL (40 nm) shows a further reduction in the ^{3}TBADN and increase in the ^{3}TPBI and ^{3}NPB signals. The trends for ^{3}TBADN and ^{3}TPBI probably indicate confinement of the recombination zone to a region near the EBL. One possible explanation of the increasing ^{3}NPB signal might be that an increasing population of ^{3}TPBI near the EBL leads to a proportional increase in the leakage of triplets through that layer. Other explanations might involve changes in the conditions at the EBL|LEL interface that affect the probability of escape of triplets or electrons. Unlike the devices for Fig. 13, those for Fig. 14 contain TBP as a fluorescent dopant in 20 nm of the ETL adjoining the LEL. In the EDEPR spectrum at 20 K, a small contribution from ^{3}TBP is hidden under the characteristic ^{3}TBADN|^{3}TCTA peak.

Figure 15 summarizes the results of this experiment and a similar experiment on the devices having varying percentages of TCTA in the LEL (devices V1−V12). The absolute intensity of the spectrum varied somewhat for extraneous reasons (e.g., positioning of the sample in the EPR cavity), but the relative intensities of the TBADN and TPBI peaks are informative. With increasing TCTA concentration or decreasing LEL thickness, the relative intensity of the TBADN peak increases. Similar trends are observed at room tempera-

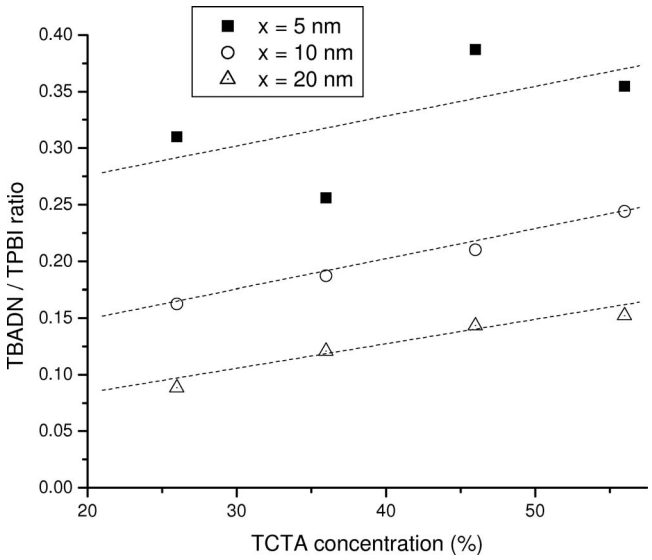

FIG. 15. Relative heights of peaks representing ^{3}TBADN and ^{3}TPBI in devices with varying percentages of TCTA in the LEL, parametric in thickness of the LEL. Organic layers are NPB|TCTA|TCTA +TPBI|TBADN:TBP|TBADN|Bphen (Table VI, devices V1−V12).

ture for the TBP component of the EL spectra (Figs. 10 and 11). The hole current passing completely through the LEL, in its dependence on TCTA concentration and LEL thickness, is most likely responsible for the trends in both the EDEPR and the EL.

All of the above EDEPR spectra were obtained at 20 K. At higher temperatures, the signals become weaker. Even so, what usually limits the temperature range is the onset of severe electrical noise. Occasionally, it is possible to extend the temperature range much closer to room temperature. Sample data are shown in Fig. 16. The devices are the same as in Fig. 15. At 20 K, the ^{3}TBP signal is hidden under the ^{3}TBADN signal, even though TBP should be a triplet trap relative to TBADN. At higher temperatures, however, the

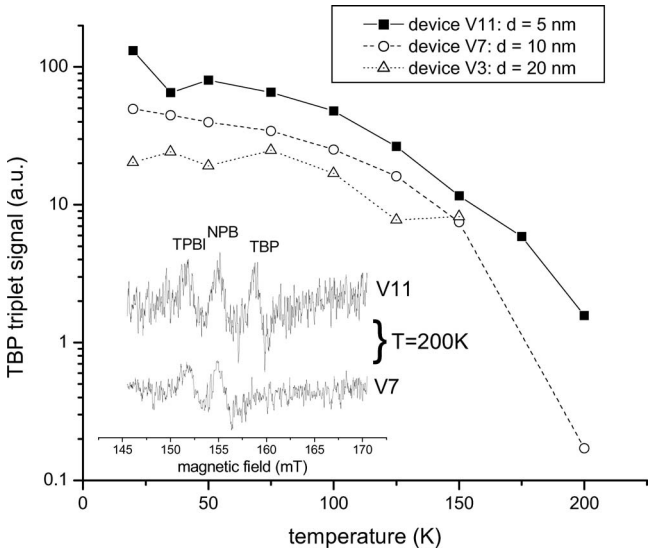

FIG. 16. ^{3}TBP signal intensity for devices V3, V7, and V11 (Table VI) with LEL thicknesses of 20, 10, and 5 nm, respectively, as a function of measurement temperature. The inset shows EDEPR spectra of devices V7 and V11 measured at 200 K.

^{3}TBADN signal disappears, perhaps because triplets become mobile enough to find the TBP traps and ^{3}TBP becomes the dominant triplet signal from the ETL. As Fig. 16 shows, the ^{3}TBP EDEPR signal decreases by more than two orders of magnitude from 20 to 200 K, but the ordering of the ^{3}TBP intensities among the three samples with different LEL thicknesses remains the same. The inset shows EDEPR spectra, measured at 200 K, of the devices with 5 and 10 nm LEL thicknesses, respectively. The ^{3}TPBI and ^{3}NPB signals in the two spectra are similar but the sample with the thicker LEL exhibits much less ^{3}TBP signal, consistent with the data at 20 K. Thus, the EDEPR data at 200 K are again consistent with the trend of the EL spectra at room temperature.

We have pointed out several parallels between the EDEPR results at low and intermediate temperatures and the EL at room temperature. The most striking EDEPR result, for which we have no corresponding information at room temperature, is the strong ^{3}NPB signal and its implication of electron or triplet leakage through the nominally blocking TCTA layer.

IV. CONCLUSIONS

We have demonstrated that efficient low-voltage PHOLEDs can be realized by use of a mixed-host composition in the LEL. Relative to a conventional neat host, a mixed host can have a shallower HOMO and a deeper LUMO while maintaining a sufficiently high triplet energy. The relative hole- and electron-transporting propensities of the mixed host can be optimized by varying the ratio of the components. The low voltage does not require doping of the charge-transport layers. For use at high current density, however, the already low voltages could be reduced even further (by $\sim$0.8 V at 20 mA/cm^2) by such doping.

The recombination zone in a representative device was found to be concentrated within $\sim$10 nm of the EBL. For this reason, the adjoining ETL does not need to have hole- or triplet-blocking properties. The voltage budget of a representative device was analyzed in detail, and the results point to opportunities for further improvement. The behavior of analogous undoped devices was discussed briefly. The emitting species is a TPBI/TCTA exciplex. EDEPR was used to study the behavior of doped and undoped devices at cryogenic temperature, which largely mimics the behavior of the same devices at room temperature. The possibility of extending the method toward room temperature was demonstrated, and the qualitative observations remained the same. Further studies of mixed-host PHOLEDs using the optical, electrical, and EDEPR methods developed here are in progress.

The mixed-host strategy is expected to improve the operating lifetime of the PHOLEDs by broadening the recombination zone, diluting chemical degradation products, and spreading the load of deleterious chemical reactions over many molecular layers. Up to threefold improvements have indeed been achieved, but much more is required for a display or lighting application. Much more stable cohost materials will probably be required. The mixed-host strategy

should greatly widen the field of possible materials by placing fewer requirements on the physical properties of the individual cohost materials.

ACKNOWLEDGMENTS

The authors thank Dr. A. P. Marchetti, Dr. S. C. Switalski, Dr. E. S. Brandt, and Dr. L.-S. Liao for photophysical measurements, and Dr. J. D. Shore for help with optical modeling. We acknowledge many helpful discussions and material research contributions of Professor C. W. Tang, Dr. V. V. Jarikov, Dr. S. Huo, Dr. X. Ren, Dr. T. L. Royster, and Mrs. B. Owczarczyk. The authors thank D. L. Comfort, D. A. Prosperi, R. S. Cupello, R. L. Winter, D. J. Neill, and D. R. Arnold for device fabrication and testing. Support and encouragement from Dr. S. Krishnamurthy is gratefully acknowledged.

[1]M. A. Baldo, D. F. O'Brien, Y. You, A. Shoustikov, S. Sibley, M. E. Thompson, and S. R. Forrest, Nature (London) **395**, 151 (1998).
[2]D. Tanaka, H. Sasabe, Y.-J. Li, S.-J. Su, T. Takeda, and J. Kido, Jpn. J. Appl. Phys., Part 2 **46**, L10 (2007).
[3]S. Watanabe, N. Ide, and J. Kido, Jpn. J. Appl. Phys., Part 1 **46**, 1186 (2007).
[4]V. I. Adamovich, S. R. Cordero, P. I. Djurovich, A. Tamayo, M. E. Thompson, B. W. D'Andrade, and S. R. Forrest, Org. Electron. **4**, 77 (2003).
[5]G. He, O. Schneider, D. Qin, X. Zhou, M. Pfeiffer, and K. Leo, J. Appl. Phys. **95**, 5773 (2004).
[6]M. Hack, M. S. Weaver, V. Adamovich, R. C. Kwong, M. H. Lu, and J. J. Brown, Proc. SPIE **5961**, 596102 (2005).
[7]K. Goushi, R. Kwong, J. J. Brown, H. Sasabe, and C. Adachi, J. Appl. Phys. **95**, 7798 (2004).
[8]Y. Shirota and H. Kageyama, Chem. Rev. (Washington, D.C.) **107**, 953 (2007).
[9]G. He, K. Walzer, M. Pfeiffer, K. Leo, R. Pudzich, and J. Salbeck, Proc. SPIE **5519**, 42 (2004).
[10]G. He, M. Pfeiffer, K. Leo, M. Hofmann, J. Birnstock, R. Pudzich, and J. Salbeck, Appl. Phys. Lett. **85**, 3911 (2004).
[11]A. B. Chwang, R. Kwong, and J. J. Brown, Proc. SPIE **4800**, 55 (2003).
[12]G. Lei, L. Wang, and Y. Qui, Jpn. J. Appl. Phys., Part 2 **43**, L1226 (2004).
[13]V. V. Jarikov, R. H. Young, J. R. Vargas, C. T. Brown, K. P. Klubek, and L.-S. Liao, J. Appl. Phys. **100**, 094907 (2006).
[14]C. Adachi, R. Kwong, and S. R. Forrest, Org. Electron. **2**, 37 (2001).
[15]K. P. Klubek and C. W. Tang, Proceedings of the ELN 2004 12th International Workshop on Inorganic and Organic Electroluminescence, 2004 (unpublished), p. 13.
[16]J.-H. Lee, H.-H. Tsai, M.-K. Leung, C.-C. Yang, and C.-C. Chao, Appl. Phys. Lett. **90**, 243501 (2007).
[17]R. J. Holmes, B. W. D'Andrade, S. R. Forrest, X. Ren, J. Li, and M. E. Thompson, Appl. Phys. Lett. **83**, 3818 (2003).
[18]Z. Popovic, H. Aziz, C. P. Tripp, N.-X. Hu, A. M. Hor, and G. Xu, Proc. SPIE **3476**, 68 (1998).
[19]Z. Popovic and H. Aziz, IEEE J. Sel. Top. Quantum Electron. **8**, 362 (2002).
[20]T. K. Hatwar, C. T. Brown, L. Cosimbescu, M. L. Ricks, J. P. Spindler, W. Begley, and J. R. Vargas, Proc. SPIE **5519**, 1 (2004).
[21]R. Kwong, M. G. Hack, T. Zhou, J. J. Brown, and T. D. Ngo, U.S. Patent No. 6,803,720 B2 (2004).
[22]T. D. Anthopoulos, J. P. J. Markham, E. B. Namdas, I. D. W. Samuel, S.-C. Lo, and P. L. Burn, Appl. Phys. Lett. **82**, 4824 (2003).
[23]S. H. Kim, J. Jang, and J. Y. Lee, Appl. Phys. Lett. **91**, 083511 (2007).
[24]S. H. Kim, J. Jang, K. S. Yook, and J. Y. Lee, Appl. Phys. Lett. **92**, 023513 (2008).
[25]C. T. Brown, J. C. Deaton, D. W. Place, M. E. Kondakova, and D. Y. Kondakov, SID Int. Symp. Digest Tech. Papers **36**, 850 (2005).
[26]M. E. Kondakova, J. C. Deaton, D. Y. Kondakov, T. D. Pawlik, R. H. Young, C. T. Brown, and D. J. Giesen, SID Int. Symp. Digest Tech. Papers **38**, 837 (2007).
[27]J. C. Deaton, D. W. Place, C. T. Brown, M. Rajeswaran, and M. E. Kondakova, Inorg. Chim. Acta **361**, 1020 (2008).
[28]L. S. Hung, L. R. Zheng, and M. G. Mason, Appl. Phys. Lett. **78**, 673 (2001).
[29]L. S. Hung, C. W. Tang, and M. G. Mason, Appl. Phys. Lett. **70**, 152 (1997).
[30]M. G. Mason, C. W. Tang, L.-S. Hung, P. Raychaudhuri, J. Madathil, D. J. Giesen, Y. Yan, Q. T. Le, Y. Gao, S.-T. Lee, L. S. Liao, L. F. Cheng, W. R. Salaneck, D. A. dos Santos, and J. L. Brédas, J. Appl. Phys. **89**, 2756 (2001).
[31]G. G. Malliaras, J. R. Salem, P. J. Brock, and J. C. Scott, J. Appl. Phys. **84**, 1583 (1998).
[32]R. N. Marks, J. J. M. Halls, D. D. C. Bradley, R. H. Friend, and A. B. Holmes, J. Phys.: Condens. Matter **6**, 1379 (1994).
[33]B. W. D'Andrade, S. Datta, S. R. Forrest, P. Djurovich, E. Polikarpov, and M. E. Thompson, Org. Electron. **6**, 11 (2005).
[34]A. P. Marchetti, private communication (August 6, 2001).
[35]A. P. Marchetti and D. R. Kearns, J. Am. Chem. Soc. **89**, 768 (1967).
[36]J. B. Birks, *Photophysics of Aromatic Molecules* (Wiley, New York, 1970), Sec. 4.2.
[37]S. L. Murov, I. Carmichael, and G. L. Hug, *Handbook of Photochemistry*, 2nd ed. (Dekker, New York, 1993).
[38]A. D. Becke, Phys. Rev. A **38**, 3098 (1988).
[39]P. J. Stephens, F. J. Devlin, C. F. Chabalowski, and M. J. Frisch, J. Phys. Chem. **98**, 11623 (1994).
[40]M. J. Frisch, G. W. Trucks, H. B. Schlegel *et al.*, GAUSSIAN 98, Revision A9, Gaussian, Inc., Pittsburgh, PA, 1998.
[41]M. J. Frisch, G. W. Trucks, H. B. Schlegel *et al.*, GAUSSIAN 03, Revision B.05, Gaussian, Inc., Pittsburgh, PA, 2003.
[42]PQS, 3.1 ed., Parallel Quantum Solutions, 2013 Green Acres Road, Fayetteville, Arkansas 72703, 2004.
[43]Jaguar 5.5, release 11, Schrödinger, Inc., Portland, Oregon, 2003.
[44]P. J. Hay and W. R. Wadt, J. Chem. Phys. **82**, 299 (1985).
[45]M. M. Francl, W. J. Petro, W. J. Hehre, J. S. Binkley, M. S. Gordon, D. J. DeFrees, and J. A. Pople, J. Chem. Phys. **77**, 3654 (1982).
[46]W. J. Hehre, R. Ditchfield, and J. A. Pople, J. Chem. Phys. **56**, 2257 (1972).
[47]R. E. Easton, D. J. Giesen, A. Welch, C. J. Cramer, and D. G. Truhlar, Theor. Chim. Acta **93**, 281 (1996).
[48]C. P. Andrieux, A. Le Gorande, and J.-M. Savéant, J. Am. Chem. Soc. **114**, 6892 (1992).
[49]H. D. Burrows, M. Fernandes, J. Seixas de Melo, A. P. Monkman, and S. Navaratnam, J. Am. Chem. Soc. **125**, 15310 (2003).
[50]M. Cölle, C. Gärditz, and M. Braun, J. Appl. Phys. **96**, 6133 (2004).
[51]T. Watanabe, K. Nakamura, S. Kawami, Y. Fukuda, T. Tsuji, T. Wakimoto, and S. Miyaguchi, Proc. SPIE **4105**, 175 (2001).
[52]V. V. Jarikov, D. Y. Kondakov, and C. T. Brown, J. Appl. Phys. **102**, 104908 (2007).
[53]R. C. Kwong, M. R. Nugent, L. Michalski, T. Ngo, K. Rajan, Y.-J. Tung, M. S. Weaver, T. X. Zhou, M. Hack, M. E. Thompson, S. R. Forrest, and J. J. Brown, Appl. Phys. Lett. **81**, 162 (2002).
[54]M. Pfeiffer, K. Leo, X. Zhou, J. S. Huang, M. Hofmann, A. Werner, and J. Blochwitz-Nimoth, Org. Electron. **4**, 89 (2003).
[55]S. Berleb, W. Brütting, and G. Paasch, Org. Electron. **1**, 41 (2000).
[56]D. Y. Kondakov, J. R. Sandifer, C. W. Tang, and R. H. Young, J. Appl. Phys. **93**, 1108 (2003).
[57]J. D. Jackson, *Classical Electrodynamics*, 3rd ed. (Wiley, New York, 1999), Sec. 6.6.
[58]O. H. Crawford, J. Chem. Phys. **89**, 6017 (1988).
[59]K. B. Kahen, Appl. Phys. Lett. **78**, 1649 (2001).
[60]V. V. Jarikov, J. Appl. Phys. **100**, 014901 (2006).
[61]G. Li, C. H. Kim, P. A. Lane, and J. Shinar, Phys. Rev. B **69**, 165311 (2004).
[62]C. F. O. Graeff, G. B. Silva, F. Nuesch, and L. Zuppiroli, Eur. Phys. J. E **18**, 21 (2005).